FOG

Freiberg Online Geoscience

FOG is an electronic journal registered under **ISSN 1434-7512**

2018, VOL 51




Broder Merkel (Ed.)

FOG special volume: Water – 3 case studies

77 pages, 3 contributions

List of contents

The images on the cover page were taken by Broder Merkel

Upper images: Impressions from field work in Bangladesh
Lower images: Field work in Mosambique

Local hydrostratigraphy, hydrochemistry and groundwater modeling in an arsenic-affected area in Bangladesh

Wael Kanoua* — Institute of Geology, Technische Universität Bergakademie Freiberg, Gustav-Zeuner Str. 12, 09599 Freiberg, Germany.
Chemical and Petroleum Engineering Faculty, AL Baath University, Homs, Syria.
Email: wael_kanoua@yahoo.com

Broder Merkel — Institute of Geology, Technische Universität Bergakademie Freiberg, Gustav-Zeuner Str. 12, 09599 Freiberg, Germany.

Abstract: An interpretation of the local scale hydrostratigraphy for an area of 107 km^2 in Titas Upazila in Bangladesh is presented. The vertical distribution of environmental tracers (chloride "Cl" and bromide "Br") and carbon isotopes (^{13}C and ^{14}C) was also investigated. Moreover, a groundwater flow model was developed for part of the area to show the local scale flow field. The region of interest (ROI) is affected by arsenic (As) contamination in groundwater (concentration > 50 µg/L). A hydrostratigraphic model demonstrates the presence of three continuous sand aquifers separated or partly separated by clay and silty clay aquitards. The upper aquifer has almost a continuous thickness throughout the model area and extends to 70-100 meters below ground level (mbgl). The second aquifer extends from ~90 mbgl to 140 mbgl, and it is connected in some parts with the coarse-sand aquifer located underneath, where the confining layer vanishes. The upper two aquifers show a slightly sloping trend toward the west. The confining silty clay or clay layers do not have the same thickness all over their extensions in the area. Discontinuous clay layers locally divide the near-surface aquifer into several laterally connected corridors. Compartmentalizing the shallow unconfined aquifer into smaller groundwater bodies by silt-clay layers might support the idea of direct recharge from precipitation rather than through leaking from ponds and/or rivers. The results of the chemical tracers show a concomitant release of Cl, Br, and dissolved organic carbon (DOC) with an increasing trend with depth. A significant positive correlation ($r = 0.8$, $p \leq 0.01$) between Br and DOC points to peat deposits (microbial mediated dehalogenation of natural organo-bromine compounds) as a potential source of their release. The conceptual flow model of part of the ROI was developed based on the observed topography and inferred hydrostratigraphy. The results of the flow model suggest the

existence of local scale flow net and the directions of groundwater flow from the manmade features toward the low-lying areas.

Keywords: Hydrostratigraphy, Arsenic, Groundwater flow modeling, Titas

1. INTRODUCTION

Groundwater contamination with As is an international problem (Eiche et al. 2008; Winkel et al. 2008; Bundschuh et al. 2010; Al Lawati et al. 2012), which has become apparent for more than three decades. Many countries around the world are suffering from this problem, especially in Asia and South America (Chowdhury et al. 2000; Rowland et al. 2006; Singh and Gupta 2008; Chakraborti et al. 2009; Roychowdhury 2010). The extent of this problem in Bangladesh is considered, according to the World Health Organization (WHO), the biggest distress affecting the human race ever (Smith et al. 2000; Ravenscroft et al. 2005; Biswas et al. 2014); it was the result of switching from surface water contaminated with bacteria as the main source of potable water to groundwater naturally contaminated with As (Dowling et al. 2002; Swartz et al. 2004; Harvey et al. 2006; Hossain 2006; Hoque et al. 2009). Bangladesh is one of the most afflicted regions as around 35 % of the population of Bangladesh is exposed to high levels of As through drinking and cooking with As-contaminated groundwater, and one-fifth of the death toll is a result of this exposure (Argos et al. 2010).

Since As discovery in groundwater in Bangladesh, a huge number of research projects has been done and more efforts have been devoted to clarify and describe the reasons behind it, to determine the factors that might play a role in exaggerating or hindering its extent (van Geen et al. 2003; Cheng et al. 2005; Aziz et al. 2008; Hoque et al. 2009; Shamsudduha et al. 2009; Planer-Friedrich et al. 2012; Hossain and Piantanakulchai 2013; Mailloux et al. 2013; Uddin and Kurosawa 2014). In general, there is consensus that the highly As-contaminated groundwater is linked to the shallow aquifer of Holocene age with gray sand, and a deep reddish-brown sand aquifer is very rarely contaminated (Horneman et al. 2004; Ravenscroft et al. 2005; Zheng et al. 2005). However, some studies presented evidence of high As concentration in the groundwater from the deeper aquifer from the Pleistocene age (Planer-Friedrich et al. 2012), or showed that this aquifer might turn, in some parts, into a source of As-contaminated groundwater in the coming future as a result of some activities (Michael and Voss 2008; Burgess et al. 2010; Radloff et al. 2011).

It is highly agreed that reductive dissolution of As-loaded Fe-oxides driven by organic carbon (OC) is the main source of As in groundwater. However, the most important and controversial issue is the source and pathway of OC as the main trigger of As release (Neumann et al. 2010; Planer-Friedrich et al. 2012; Whaley-Martin et al. 2016), especially nowadays as OC of both labile and recalcitrant forms has been proven to enhance As release by several mechanisms (e.g., electron donor, complexation, competitive sorption, and electron shuttling) (Mladenov et al. 2010; Mladenov et al. 2015; Kulkarni et al. 2016). In the shallow aquifers, many studies reported a vexing spatial variability of As concentration in groundwater in Bangladesh (van Geen et al. 2003; Shamsudduha 2007), and temporal variability was reported in other studies in Bangladesh (Planer-Friedrich et al. 2012) and West Bengal (Majumdar et al. 2002; Savarimuthu et al. 2006; Tathagata and Rolee 2011). This bewildering availability and distribution was attributed to different factors (groundwater chemistry, topography, lithology, recharge, and flow regime). However, recent studies emphasized the role of geological structure and specially the irregularly distributed fine-grained channel-fill sediments (silt-clay layers) in the subsurface (Eiche et al. 2008; Desbarats et al. 2014) and the underground palaeosol (McArthur et al. 2008; McArthur et al. 2011; Hoque et al. 2012, 2014; Ghosal et al. 2015). Moreover, the topography also plays an essential role in this regard (Hossain and Piantanakulchai 2013; Khan et al. 2016), in which it might influence the groundwater flow and redistribution of contaminants in the underground. So the question is how to link underground geology with the surface topography to As release and distribution in the subsurface.

In this study, the shallow hydrostratigraphic framework in an As-affected region of the central eastern part in Bangladesh was investigated by a mean of three-dimensional (3D) lithological model to get deep insight into the area. Moreover, environmental tracers and carbon isotopes were used to track the possible source of OC. Flow modeling wss also conducted to study the subsurface flow net.

2. REGION OF INTEREST (ROI) AND BACKGROUND

2.1. Region of interest

The ROI is shown in Figure 1. It comprises ~107 km^2 of the As-affected area in Comilla district of Chittagong division, Bangladesh. About 170,000 people reside in this area, and the core crop is paddy. The ROI is located on the Meghna flood plain, and bordered by Homna to the north, Daudkandi to the south, Muradnagar to the east, and Meghna to the west. Naturally,

it is bounded by the main channel of the River Meghna in the west, the River Gumti in the south and east, and the River Titas in the north. These rivers are considered the most important geomorphic features in the ROI.

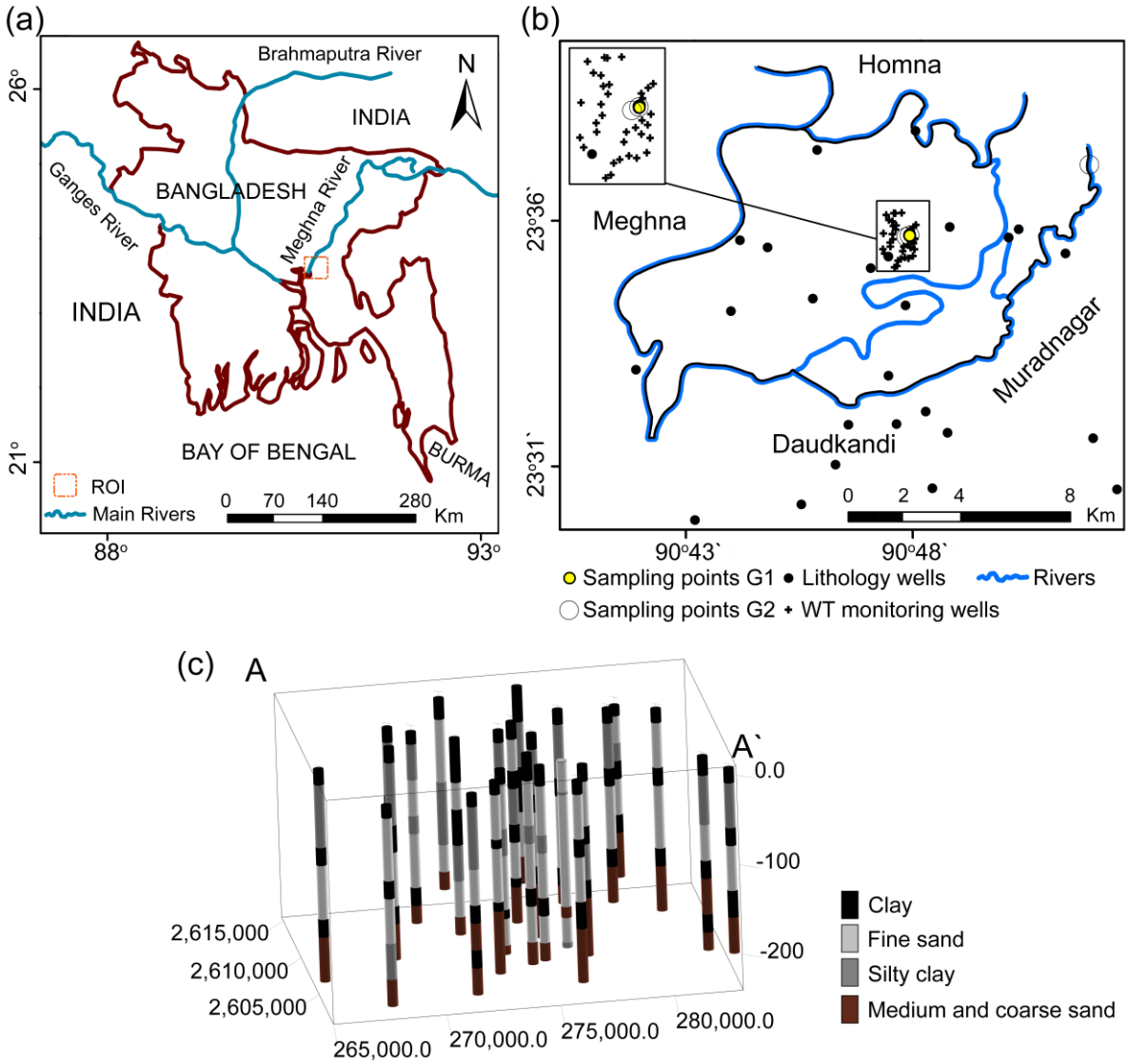

Figure 1 (a) Map of Bangladesh with the main rivers and the neighboring countries, showing the location of the ROI (red dashed rectangle) within Bangladesh, (b) the extent of the lithology model and the important rivers plus lithology wells (black dots), ^{14}C and ^{13}C sampling wells (G2: empty circles), water table monitoring wells (black crosses), and chemical components sampling wells (G1: yellow dots) within the ROI, and (c) 3D strip-logs showing the lithology in each borehole

In general, the topography of the ROI is more or less flat (maximum elevation of about 25 meters above sea level (masl) in the northern part and sloping toward the outlet of the Meghna basin), with a gradient of ~0.4 m/km from north to south. The most salient topographic features of the ROI are the artificially raised areas for settlements and villages (e.g.,

embankments and mounds that houses are built on above the flooding level) (Kanoua and Merkel 2017), which are typical features elsewhere in Bangladesh (Harvey et al. 2006; Maitra et al. 2014). In order to obtain detailed elevations, a digital elevation model (DEM) was acquired from the Consultative Group for International Agriculture Research Consortium for Spatial Information SRTM C-band CGIAR-CSI v4.1 with a spatial resolution of 3 arc-sec and processed regarding the missing topographic features in the ROI (Kanoua and Merkel 2015).

2.2. Background

2.2.1. Geological settings

A map of Titas Upazila with the well's location is shown in Figure 1. The ROI has sediments of both the Holocene and Pleistocene ages (Planer-Friedrich et al. 2012). Due to frequent riverbed migrations, the aquifers are not fully separated and in some locations seem to be connected by sand lenses (as inferred later from cross sections).

The Meghna floodplain, where the ROI is located, is characterized by highly As-contaminated aquifers, which are situated in the late Pleistocene-Holocene peat layers, silty sand, and clayey silt deposits (Acharyya et al. 2000). During the peak of the last ice age (around 18000 years ago) the major rivers cut deep valleys into the sediments (Anawar et al. 2011), and during the mid-Holocene Climatic Optimum, extensive peat deposits accumulated (Umitsu 1993). Nowadays, almost all the highly As-contaminated groundwater occurs in the sediments deposited at that time, while the sediments covering the low sea level are bearing As-free groundwater (Acharyya et al. 2000; Saunders et al. 2008).

2.2.2. Groundwater flow

Due to the low topographic gradients in the ROI the hydraulic gradient is expected to be very small, commonly 0.0001. The lateral groundwater flow in the shallow aquifer is very slow, and the Darcy velocity is about 2 m/a as an overall value in the Bengal basin (Burgess et al. 2002). It is postulated that the flow system on the local scale exists between local topographic features (elevated residence areas, levees, flooded depressions, minor rivers) to a depth of about 10-30 m. Moreover, groundwater pumped for domestic, industrial, and irrigation uses might disturb the natural flow systems considerably, especially affecting the vertical components of flow.

3. DATA AND METHODOLOGY

Lithologic data for this study were collected from 25 lithologs of drinking and irrigation wells, plus seven observation wells as shown in Figure 1. The depths of the lithologs range from 10 to 240 mbgl (mean 177 and median 220 mbgl). They are distributed throughout the ROI (horizontal spacing varies between a few meters to ~18 km). The lithology of the logs was provided in tabulated form and consists of three major types of unconsolidated sediments: clay, silty clay, and sand. A number of lithologs recorded further subdivisions of the sands in terms of grain size (fine, medium, and coarse sand). More detailed information on the color and grain size of the sediments was just mentioned in the monitoring wells. No soil horizon was mentioned to cover the ROI; however, at the site of the monitoring wells (Titas hospital complex and its access road), there is a base foundation consisting of alternating layers of sandy material and plastic sheeting (Planer-Friedrich et al. 2012). From a general hydrogeological point of view, the sediments have been categorized as aquifers (sand) and aquitards (clay). The position of the silty clay is also considered to act as an aquitard. The extent, thickness, and hydraulic conductivity of these clay or aquitard layers are very important as they govern the 3D flow of groundwater at the local and regional scales.

Groundwater and surface water analysis data are derived from different sources. Chemical tracers (Cl and Br) data are from six individual monitoring wells (this group of samples is referred to later as G1) drilled in 2007 in the ROI (depth: 9-85 m) for the purpose of hydrogeochemical monitoring with depth (Planer-Friedrich et al. 2012). The results of the ^{14}C and ^{13}C of dissolved inorganic carbon DIC ($^{14}C_{DIC}$) and ($^{13}C_{DIC}$), respectively, are from Hoque and Burgess (2012). They collected, in 2008, many groundwater samples, four of which were located in the ROI (this group of samples is referred to later as G2). These samples were from domestic and monitoring wells in the Titas area (depth: 15-336 m). The data from the surface water and rain water analysis are taken from Ahmed et al. (2010) and Sultana (2007), respectively.

The data for the groundwater flow model application were collected from the physical parameters and hydrogeological properties of the aquifer. The model domain was identified, and the model conditions were determined using the hydrological and geological data. The measured water levels at a number of monitoring wells were prescribed at these boundaries. The model was calibrated for steady state by trial and error. The flow paths were analyzed through the model domain according to the velocity field and flow directions.

4. RESULTS AND DISCUSSION

4.1. Lithologic modeling

According to the author's knowledge, hydrostratigraphical modeling work has not been done on a local scale in the ROI. All of the already available reports provide just a brief description of the lithology without concentrating on the relations between the individual sedimentary facies on the local scale.

RockWorks (RW) version 2004® (RockWare, Golden, Colo., USA) and the available lithologs were used to develop the 3D lithological model of the ROI. The sedimentary sequence is overlain in many parts by clay, as found elsewhere in Bangladesh. The thickness of the top clay varies throughout the ROI. The topographic elevation corresponding to each well was extracted from the DEM, modified to represent the topographic surface with all the features.

The model was run after importing all the wells with their corresponding lithology intervals (top and base) in RW. The interpolation between the well logs in 3D was conducted by the algorithm of "lithoblending". Each voxel is assigned a lithology value corresponding to a particular lithotype of the closest known data point and then the processes continue both horizontally and vertically to the next voxel and so on, until a voxel with a specified lithology value (that is the next known data point) is encountered.

The sensitivity and validation of the 3D model was carried out as proposed by Mukherjee et al. (2007). Optimization was conducted by changing the node spacing of the model and testing how the model reacts. The model, which showed the least change toward the change in grid size was selected as final one. Verification was carried out using two well logs, which were excluded during building the 3D model. The results of the model optimization showed the model as being stable at a spacing of 100 × 100 × 2 m in the x, y, and z directions, respectively and the verification step delivered satisfactory results by visual comparison.

Unfortunately, no detailed age and color information is available about the different lithofacies and therefore generalization and visual interpretation was used here to set the different aquifers and aquitards in the ROI. Color information is just available in some monitoring wells in the middle of the ROI, which was used here to guide and direct, to some extent, the interpretations of vertical extension of different proposed aquifers. Planer-

Friedrich et al. (2012) showed the existence of reduced sediments (gray color) to a depth of 75 m. Moreover, they stated that the second sandy layer follows the first clay and starts at a depth of 83 m and the sediment has a brown color, which reveals an oxidized state. Due to the fact that this is the only information available about the sediment color with depth, the clay layer above the brown sand is considered here to play a role of a hydraulic barrier between the upper and middle sand aquifers. This clay layer could be the laterite surface (clay layer) mentioned by Goodbred and Kuehl (2000), which was found at a depth of ~85 m in the Meghna floodplain. This surface, called palaeosol in other studies as well, plays a role in preventing downward movement of groundwater (Hoque et al. 2012; McArthur et al. 2016; Mihajlov et al. 2016). This idea, that the deeper low-As aquifer is relatively isolated from the shallow, high-As aquifer, is supported by the most recent investigations in Bangladesh and West Bengal (McArthur et al. 2016; Mihajlov et al. 2016).

The five east-west cross sections in Figure 3 (corresponding to the white traverses in Figure 2) provide a detailed representation of the underground framework as inferred from the 3D lithologic modeling.

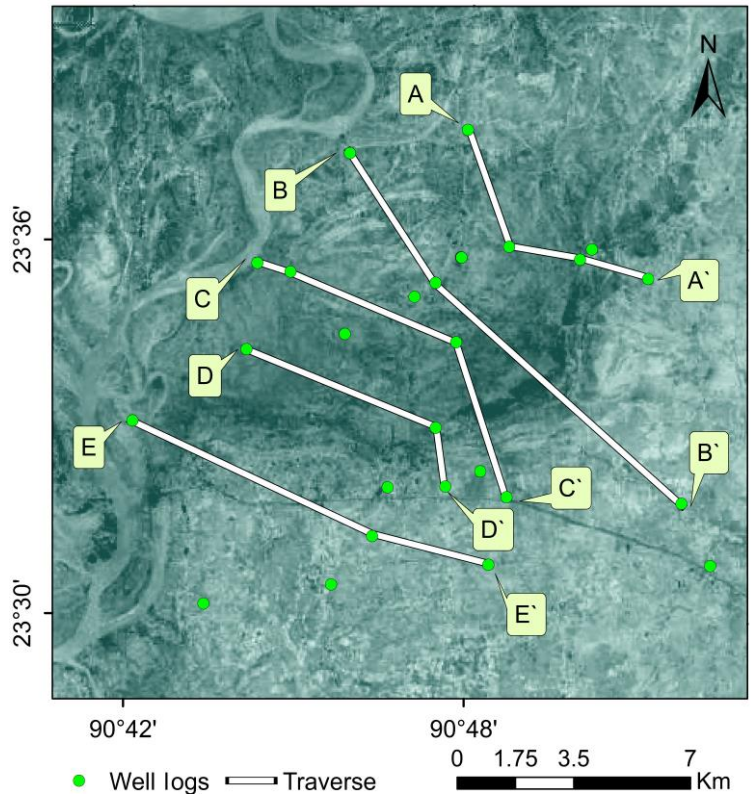

Figure 2 Locations of available boreholes (green circles), and five east-west traverses (white lines: A-A`, B-B`, C-C`, D-D`, and E-E`) shown on a background map of the ROI acquired from Google Earth 7.1.2.2041 (acquisition date: 16.06.2014)

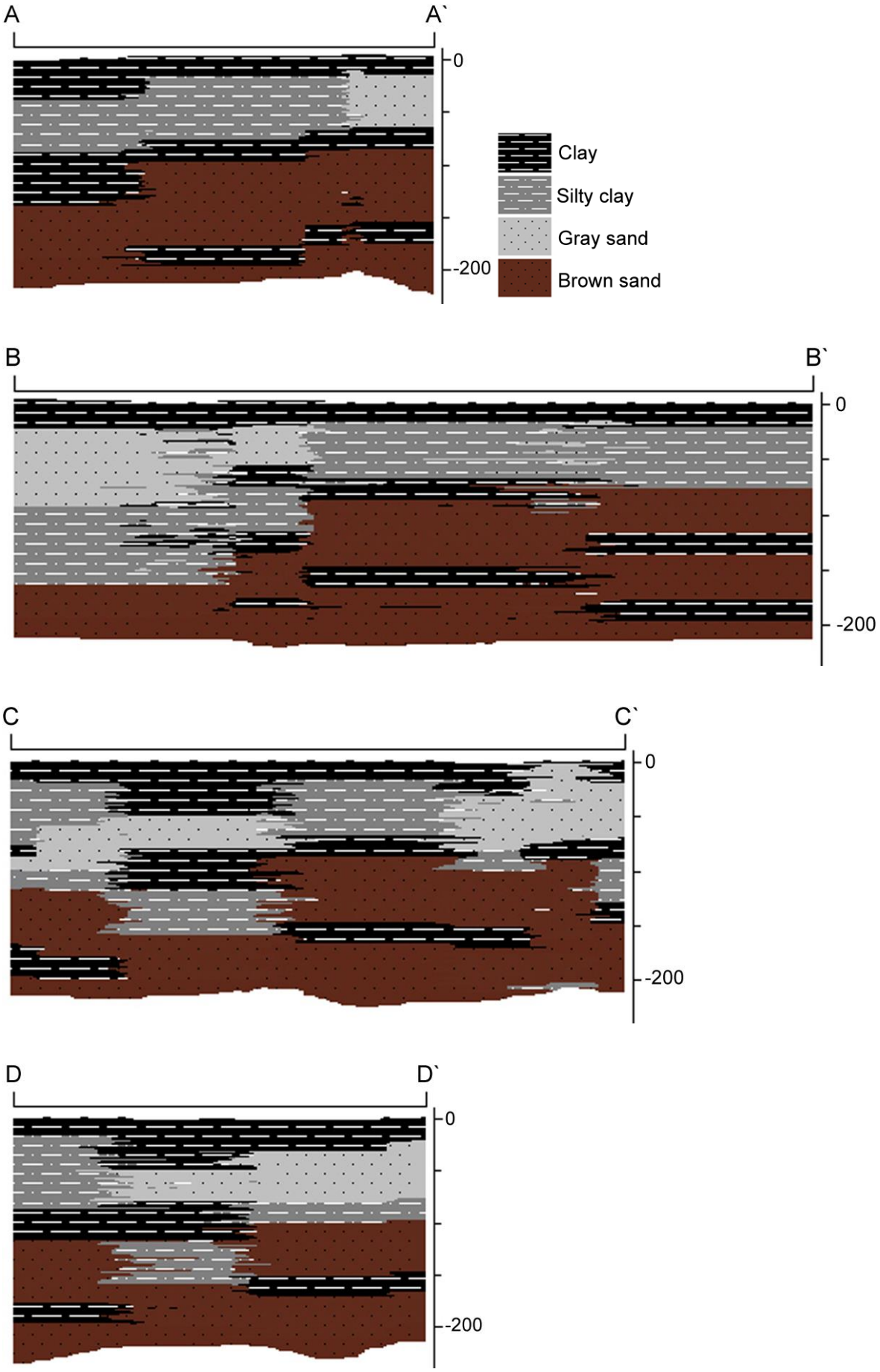
A
A`
0
-200
Clay
Silty clay
Gray sand
Brown sand
B
B`
0
-200
C
C`
0
-200
D
D`
0
-200

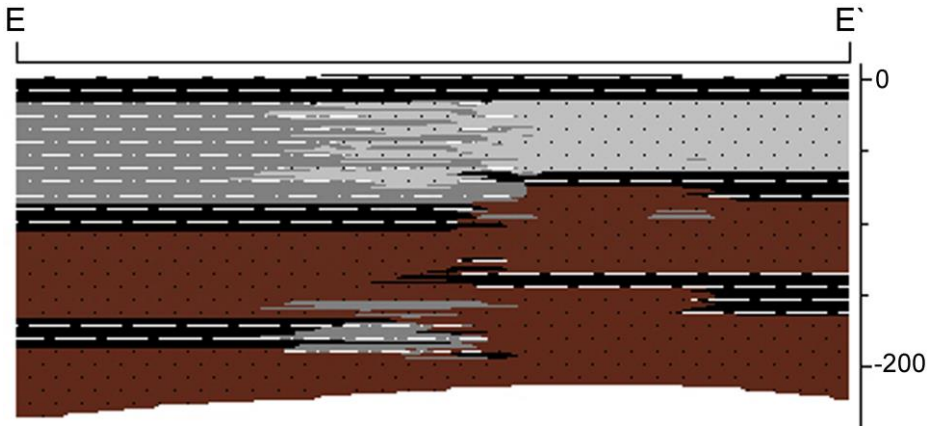

Figure 3 Modeled cross sections along transects A-A`, B-B`, C-C`, D-D`, and E-E` in Figure 2 (vertical exaggeration: 20)

All boreholes in the ROI penetrate multiple levels of sand, silt clay, and clay materials of different lateral extent. It seems from the cross sections that the underground system can be divided into three sandy units separated by two clay and/or silty-clay layers. These clay and silty-clay confining layers do not have the same thickness all over their extensions and they play the role of aquitards due to their low hydraulic conductivity. Despite lateral discontinuity, the clay and silty-clay layers could introduce a vertical hydraulic anisotropy, influencing to some extent the groundwater flow pattern (Zijl 1999; Tóth 2009). Michael and Voss (2009) reported high anisotropy values for the hydraulic representation of the aquifer at the scale of the entire Bengal Basin. Moreover, modeling efforts by Hoque and Burgess (2012) showed that the depth < 70-100 mbgl is the threshold between the shallow and deep flow systems in the Bengal Aquifer System (BAS).

The extent of the bottom sand aquifer is difficult to grasp as no wells penetrate the whole thickness of this unit. The five east-west cross sections reveal that the middle and bottom sand levels are not fully separated, rather they are connected in many parts throughout the ROI. This connectivity lets one draw the conclusion that the same conditions (oxidizing/reducing) might, to some extent, dominate in both proposed aquifers. Moreover, six plan-view maps at different depths (20, 30, 40, 50, 60, and 70 m) were created in RW and are presented in Figure 4. These maps represent the lateral distribution of the different lithofacies at different depths. A complex lateral distribution is to be inferred from the different presented plan maps.

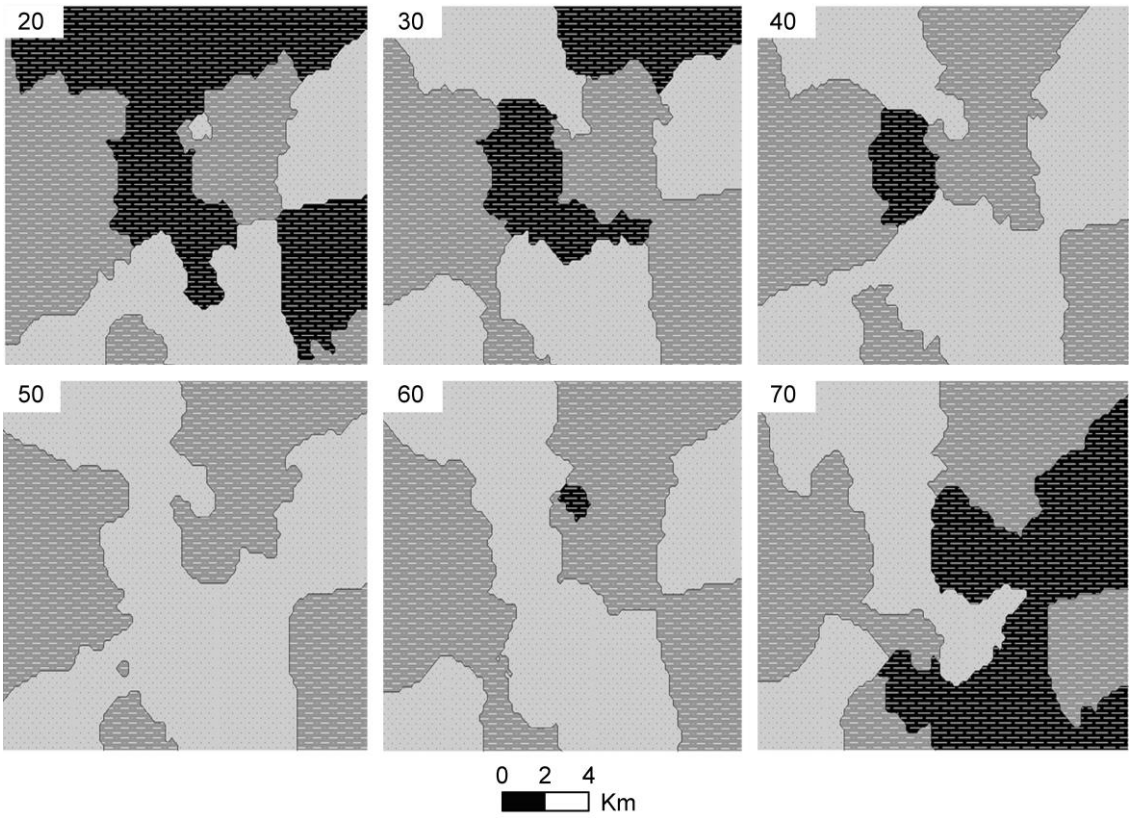

Figure 4 Plan-view maps showing the distribution of different hydrostratigraphic units at six different specific depths (20, 30, 40, 50, 60, and 70 mbgl) over the ROI

According to the previous discussion, a system of three aquifers can be proposed in the ROI. The upper aquifer is disconnected laterally throughout the model area and extends to a depth of 70 m. This aquifer is considered the highly As-contaminated aquifer, where the sediments show gray color. The second aquifer extends from ~90 m to 140 m in depth, and it is connected in some parts, where the confining layer vanishes, with the coarse-sand aquifer located underneath. The second aquifer shows a brown sediment color, indicating oxidizing conditions.

4.2. Chemical tracers and carbon isotopes (^{13}C and ^{14}C)

Despite the availability of different hypotheses, the high As concentrations in the groundwater in Bangladesh are consensually explained by the desorption of arsenate through the reductive dissolution of solid Fe-oxides and/or the reduction of sorbed arsenate to arsenite (Nickson et al. 2000; Zobrist et al. 2000; Ravenscroft et al. 2001; Islam et al. 2004; McArthur et al. 2004; Polizzotto et al. 2005; Wang and Mulligan 2006; Akai et al. 2008; Tufano and Fendorf 2008; Planer-Friedrich et al. 2012). This reductive dissolution is found to be driven by DOC in groundwater. The nature, source, and release mechanism of this DOC are still under

discussion (Neumann et al. 2010; Planer-Friedrich et al. 2012). The potential sources of labile DOC in Bangladesh aquifers include terrestrial (plant/soil) organic matter such as peat dispersed throughout the aquifer sediments (McArthur et al. 2004; Planer-Friedrich et al. 2012; Uddin and Kurosawa 2014) and surface water DOC brought to depth by natural flow or irrigation pumping (Harvey et al. 2002; Polizzotto et al. 2005; Neumann et al. 2010). Although different perspectives are available about which organic matter contributes to redox reactions in aquifer systems (Kelleher and Simpson 2006; Lehmann et al. 2008; Schmidt et al. 2011), both new and old organic matter could potentially drive such reactions (Mailloux et al. 2013), and the presence of specific enzymes in the bacterial community determines if the organic matter can be used as a substrate for metabolic processes (Ghosh et al. 2015). In the Bengal Basin, this reactivity of old organic matter in fine-grained channel-fill has also been reported (Desbarats et al. 2014).

Chloride (Cl) and bromide (Br) are conservative chemical tracers, used to track the source of contamination in groundwater (Davis et al. 1980; Davis et al. 1998). The Cl and Br concentrations of all the water samples (G1 samples) from different depths are significantly positively correlated with correlation coefficient 0.99 ($p \leq 0.01$) (Figure 5). This refers to the fact that both of them could be stemming from the same source. Vertical profiles of Br and Cl (Figure 6) show increasing trends with depth. The concentrations of Cl in surface water and rain water (green and blue vertical lines in Figure 6) are 50.5 and 15.1 mg/L, respectively. Moreover, all studies on surface water in the ROI reported negligible or zero Br in their samples (Ahmed et al. 2010). Therefore, it is impossible for Br (and Cl) to be derived from the surface (ponds/rivers). In other words, the only possible source must be in the underground.

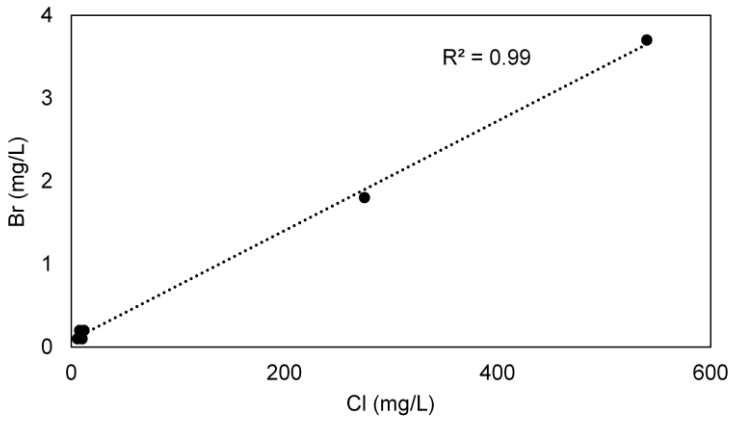

Figure 5 Cl versus Br concentrations for groundwater samples from different depths in the ROI

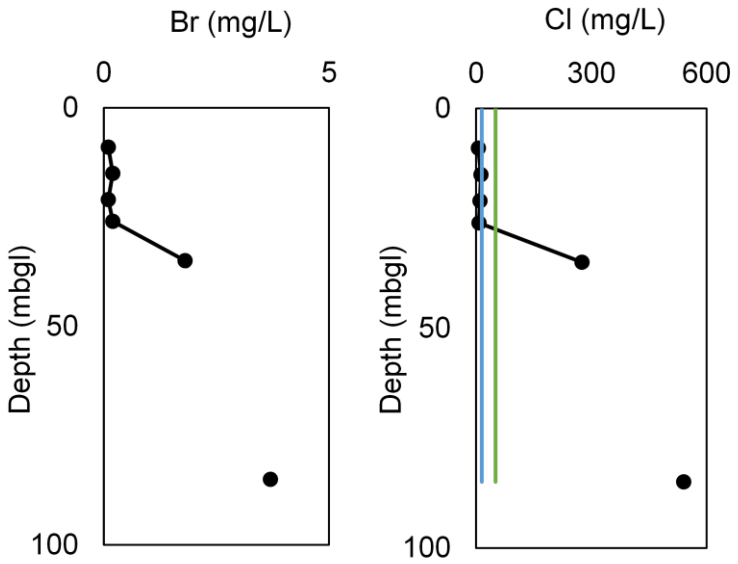

Figure 6 Cl and Br profiles with depth. Vertical blue and green lines represent Cl concentration in rain water (Sultana 2007) and surface water (Ahmed et al. 2010), respectively

Bromide and DOC (G1 samples) also show an increasing trend with depth and are significantly positively correlated ($r = 0.8$, $p \leq 0.01$) (Figure 7). Generally, Br has a positive correlation with DOC (Kabata-Pendias 2001) and especially in areas enriched in peat, where high concentrations of Br are reported to be bound in the organic form “organo-bromine” (Biester et al. 2004). Microbial mediated dehalogenation of natural organo-bromine compounds releases DOC, which is the predominant mechanism of Br release from peat (Biester et al. 2006). The same correlation between Br and DOC has been reported before (Desbarats et al. 2014), and the high correlation was explained as both constituents being decay products of natural organo-bromines and are released in/from channel-fill sediments (aquitards). This explanation seems plausible; hence it needs further investigation. On the other hand, pore water in clay/peat layers in Bangladesh is reported to contain high residual salinity of up to 12000 mg/L for TDS (Total dissolved solids) (Ravenscroft et al. 2001), and since deposition, pore water got enriched in DOC due to the long contact with the organic-rich deposits. Therefore, clay/peat layers are a potential source of DOC in the ROI.

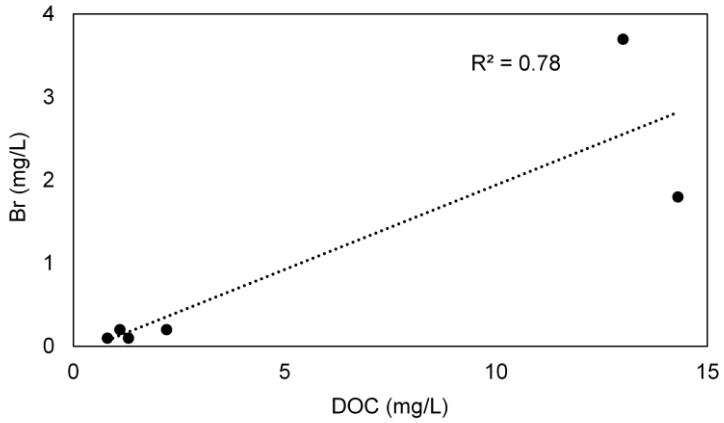

Figure 7 Br versus DOC concentrations for groundwater samples from different depths

The correlation between As from one side and Cl, Br, DOC, and TIC from another side (G1 samples) is not significant. Arsenic distribution also does not show a clear trend as other elements do (increasing/decreasing trend with depth). The release of As from peat/clay layers is therefore unlikely, at least with the available data at hand. This finding is in accordance with previous results, as As in organic matter in Bangladesh is reported to be very low (Dowling et al. 2002). Thus, the source of As is present as a dispersed element sorbed to dispersed Fe-oxides in the subsurface. So, As will not be released from Fe-oxides unless organic matter is present to drive microbial reduction; thus, the flow regime is likely to redistribute the As-release trigger (OC), which is in the end responsible for the existing distribution of As in the subsurface.

Total inorganic carbon (TIC) in groundwater consists of fluxes from atmospheric, mineral, and biological (oxidation of organic matter) sources. The influence of the atmospheric source is unlikely, at least in the ROI, as TIC is increasing with depth. It is also difficult to judge the carbonate contribution to TIC; however, the correlation between dissolved Ca plus Mg and TIC (G1 samples) is not significant. The TIC profile (up to a depth of 87.8 m) points, however, to the source being oxidation of organic matter, which is high in peat/clay layers. This is supported by the significant positive correlation between TIC and DOC ($r = 0.98$, $p \leq 0.01$).

Measurement of $^{14}C_{DIC}$ in pore water is important for studying the oxidation of OC (McNichol et al. 1994). As mentioned before, the results of $^{14}C_{DIC}$ are taken here from Hoque and Burgess (2012). Despite the limited number of samples, the $^{14}C_{DIC}$ activity, ranging from 7.07 to 104.71 pMC (percent modern carbon), shows a decreasing trend with depth (Figure 8). Hoque and Burgess (2012) calculated three groundwater ages from $^{14}C_{DIC}$ activities, using

100 pMC and 87 pMC as initial ^{14}C activity with/without considering dilution of ^{14}C due to interaction with aquifer carbonate minerals (taken as dead with respect to ^{14}C). However, carbonate minerals are in general enriched in ^{13}C (e.g., carbonate has $\delta^{13}C$ close to 0 ‰) (Cark and Fritz 1997; Singh et al. 1998). Thus, the sharp depletion of $^{13}C_{DIC}$ (> 35 %) between 87.8 m (-13.76 ‰) and 140 m (-38.57 ‰) refers to the effect of an abnormal source of depleted ^{13}C, and the effect of detrital carbonate dissolution could be ruled out. The $\delta^{13}C_{DIC}$ (-38.57 ‰) also falls far from the value expected for oxidized OC from C3 plants (-28 ‰) and C4 plants (-13 ‰) in the Bengal Basin (Sarkar et al. 2009), even after taking fractionation during plant residue decomposition into account (Schweizer et al. 1999; Wynn 2007). This ^{13}C depletion is postulated to result from the dissolution of pedogenic calcite, which could be more ^{13}C-depleted as low as -125 ‰ (Drake et al. 2015). The pedogenic calcite results as ^{13}C-depleted methanogenic methane (CH_4) (from anaerobic degradation of organic matter in carbon-rich peat/clay layers) is oxidized in-situ and the produced hydrogen carbonate reacts with Ca (reaching 66 mg/L) to form calcite. The role of CH_4 oxidization could be checked by measuring $\delta^{13}C$ in carbonate minerals found in the second aquifer (> 90 mbgl).

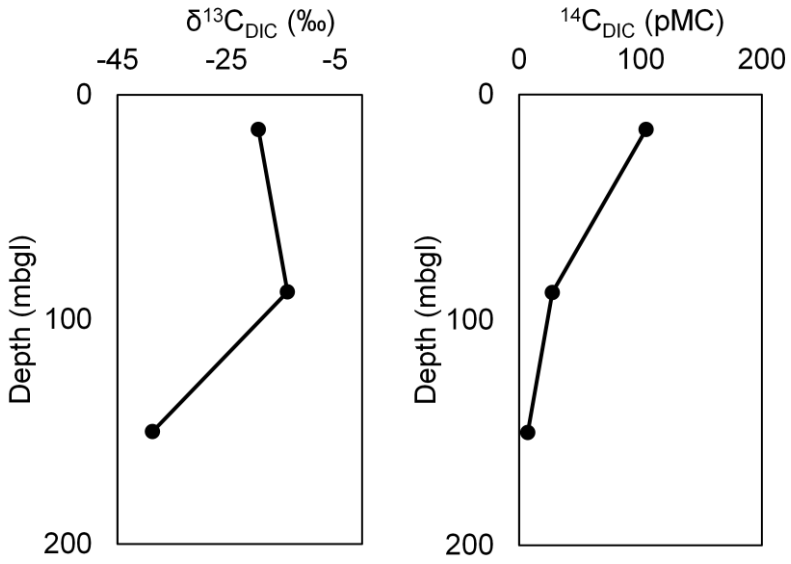

Figure 8 $^{14}C_{DIC}$ activity (right) and $\delta^{13}C_{DIC}$ (left) profiles with depth

From Figure 8, the sample from the depth of 87.8 m shows enrichment in $^{13}C_{DIC}$ (> 5 ‰) compared to the sample from the depth of 15 m (soil-CO_2), and dilution of $^{14}C_{DIC}$. The effect of detrital carbonate dissolution ($\delta^{13}C$ close to 0 ‰) is excluded here due to the reasons mentioned before. Anaerobic degradation of organic matter (in peat/clay layers) eventually results in the production of CH_4 and CO_2, and this CO_2 is more enriched in ^{13}C (Whiticar 1999), especially in comparison to soil-CO_2 (Han et al. 2014). Therefore, and recalling that

TIC increases with depth (samples G1), it is proposed that the $^{13}C_{DIC}$ profile (up to a depth of 87.8 m) is produced by the superposition of two independent carbon profiles different in ^{13}C, each is generated from a different source located at a distinct depth. These two sources could be the soil-CO_2 and methanogenesis-CO_2. Methane measurements were not conducted for the available water samples; however, ammonium (NH_4), which is an indicator of microbial activity and intensity of organic matter degradation in the anoxic groundwater (Dowling et al. 2002; Postma et al. 2007), shows an increasing trend with depth (G1 samples), and methanogenic CH_4 is normally associated with it.

The discrepancy between $^{13}C_{DIC}$ enrichment/depletion above/below the depth of 87.8 m, respectively, could be explained by the existence of shallow and deep flow systems in the BAS. Hoque and Burgess (2012) reported from modeling investigations the existence of shallow (< 70-100 mbgl) and deep (> 150 mbgl) flow systems in the eastern part of Bangladesh. The authors did not find a trend (samples > 150 mbgl) with respect to the basin's eastern margin. However, taking their analyses of all the water samples > 70-100 mbgl, Ca increases with distance from the eastern margin ($r = 0.5$, $p = 0.06$). Also Majumder et al. (2013) used borehole temperatures and concluded from deep observation wells on the eastern margin of Bangladesh that deep recharge does take place. Thus it can be postulated that the depth 70-100 m is the threshold between the shallow and deep flow systems in the BAS. Deep groundwater is recharged through the outcrops in the eastern hilly regions and shallow groundwater is recharged from the surface. Due to the slow flow and high residence time, deep groundwater gets gradually depleted with ^{13}C through dissolution of pedogenic calcite along its flow path. On the other hand, shallow groundwater circulation takes place over a time interval of less than hundred years (*Ibid*), and the two carbon pools, with different ^{13}C signatures, get mixed. The oxygen and hydrogen isotope ratios (samples G1 and G2) plot on the meteoric water line (data are not shown), indicating the origin as local precipitation, and the lower $\delta^{18}O$ (-4.21 ‰) in the deep groundwater sample is in the range reported previously for precipitation in Bangladesh (Aggarwal et al. 2000), and does not indicate climatic differences/palaeo-recharge. The case of the groundwater samples showing enrichment/depletion relative to a critical value may not exclusively indicate climatic differences, and other factors (e.g., the continental effect) need to be carefully evaluated.

The results of the chemical tracers and $^{14}C_{DIC}$ are in congruity with the previous facts and findings. Generally, the highest amounts of DOC are found in organic-rich aquitard environments (Thurman 1985). Moreover, the aquifer/aquitard interface is a very important

zone, which provides a mixing zone supporting microbial activities within the aquifers, and producing a change in the chemical composition of groundwater (McMahon 2001). Peat layers are also known to produce “tea” colored water due to the microbiological decay of the OC in these environments (Aguilar and Thibodeaux 2005). Different studies found that terrestrial (plant/soil) DOM at depth from dispersed sedimentary organic matter such as peat adds a labile substrate to fuel bacteria and maintain reducing conditions in the aquifer (Dowling et al. 2002; McArthur et al. 2004; Mladenov et al. 2010). Others showed that the presence of peat is considered to have a critical role in the occurrence of high As concentration in groundwater (Uddin and Kurosawa 2014). Other evidence also comes from stable isotopes (O), as investigations in Bangladesh and West Bengal showed that high and low-As groundwaters have different isotopic signatures (Desbarats et al. 2014; Planer-Friedrich et al. 2012). This might imply different recharge sources/paths, or groundwater is influenced by isotopic fractionation between water and organic matter when they come into contact (Chen et al. 2016). Moreover, As is found to peak at different depths, e.g., 15, 30, 55, 60, 75, and 100 (Nickson et al. 2000; McArthur et al. 2001; Ravenscroft et al. 2001; Zheng et al. 2005; Dhar et al. 2008; Tareq et al. 2013), which could be explained by the wells’ proximity to the carbon sources, with peat/clay layers being located at different depths (stratigraphic model).

Recent, surface-derived OC (e.g., water of excavated ponds, latrines, irrigation return flow) advected within the aquifer is proposed by different researchers as the main source of carbon fueling the reductive dissolution and releasing As (Harvey et al. 2002; Polizzotto et al. 2005; Neumann et al. 2010; Mailloux et al. 2013). However, groundwater contamination with As in Bangladesh and wastewater high in OC (from septic tanks and pit latrines) were shown to be inversely correlated (van Geen et al. 2011; Leber et al. 2011; McArthur et al. 2012). This points to the fact that the wastewater infiltrating downward in the aquifer does not induce As mobilization until something changes in the underground. This might be the infiltrating water passing through/near a carbon-rich source in the underground, and getting loaded with the trigger of As release. Mailloux et al. (2013) stated that advected OC from the surface controls the aquifer redox status and fuels As release in the aquifer system in Bangladesh. Their study area is characterized by high As where sand extends to the surface, and vertical infiltration is relatively high. However, recharge-induced flushing has been proposed to explain low-As concentrations at shallow depths beneath sandy surficial sediments (Stute et al. 2007; Aziz et al. 2008; van Geen et al. 2008; Weinman et al. 2008; Hoque et al. 2009). Thus, this paradoxical effect has to be investigated further. Moreover, the most As-affected areas are

located where the thick clay surficial layer exists, which slows down/impedes, to a high extent, the vertical percolation of surface water loaded with OC (Aziz et al. 2008; Weinman et al. 2008; Hoque et al. 2009). Other studies which supported the surficial source (pond water/re-infiltrating irrigation water) of carbon also reported old carbon at the depth of sampling (Harvey et al. 2002; Klump et al. 2006; Neumann et al. 2010), and this discrepancy in the carbon ages is explicable in terms of the reservoir of carbon and its derivation from older buried peat. Moreover, the supply of fresh carbon from the surface to the subsoil stimulates the microbial mineralization of older carbon (Fontaine et al. 2007). Sengupta et al. (2008) and Datta et al. (2011) showed that pond water, at least in their study areas, does not provide OC to the aquifers. Also, Klump et al. (2006) concluded, using environmental tracer data and conceptual groundwater flow and transport modeling, that re-infiltrated irrigation water is excluded from being a direct cause of As release.

4.3. Groundwater flow modeling

Modeling the evolution of the As-rich groundwater in Bangladesh with much confidence is not an easy task, if not impossible, due to its complex nature coming from the different factors affecting it. It is possible, however, to carry out some simple modeling to show how some factors affect this evolution. Based on the already presented hydrostratigraphic and chemical results, it is possible to explain the heterogeneities of As concentration using groundwater flow in combination with topography and the identified source of the OC, namely, peat silt-clay layers, that drives Fe-oxides reduction.

From the water table monitoring wells, it is clear that topographic elevation corresponds with the hydraulic head (Figure 9). The correlation test showed a significant positive correlation between the topography and the water table ($n = 43$, $r = 0.7$, $p < 0.001$). The same trend was noticed by Weinman et al. (2008) in another study in Araihazar in Bangladesh. Also, groundwater age investigations by Radloff et al. (2015) showed the presence of newer groundwater in the village (elevated area) and older groundwater closer to the discharge area (low-lying area) with an increasing trend of As and age. This refers to the fact that the local topography does have an effect on the groundwater flow. Thus, the man-made elevation sets up a higher hydraulic head and the greater potentiometric surface of the elevated areas suppresses the flow into these areas from the low-lying ones. That means, that this variation in the local topography may cause hydraulic short-circuiting of the shallow flow system, which was also proposed by other researchers (Michael and Voss 2008; Burgess et al. 2010). This

could be a plausible explanation for the fact, that adjacent wells separated by just a few meters may yield water from the same depth yet have contrasting high and low As content.

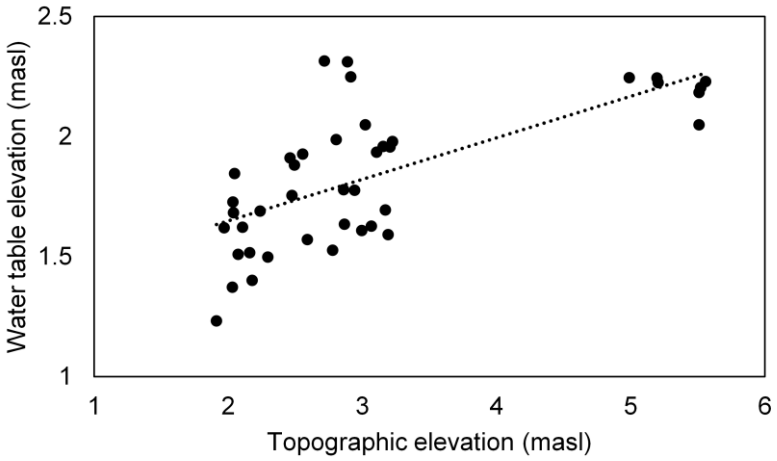

Figure 9 Correlation plot for the surface topography and water table elevation for all water table measurements in the Titas area

A 3D flow model was build up with PHAST. Boundary conditions (front and side boundaries) were set to specified head boundary conditions according to the measured head in the margin wells. Dispersivity and hydraulic conductivity values were taken from Planer-Friedrich et al. (2012). The values of hydraulic conductivity in the aquifer and evapotranspiration (as flux boundary conditions) are adjusted with a view to obtaining the observed hydraulic head data. Groundwater flow was modeled as steady state. The weighting parameters used by PHAST for the space and time differencing were left as the default values 0 and 1, respectively.

Figure 10 shows the modeled groundwater flow velocity vectors. The model shows the horizontal and vertical flow patterns (streamlines) at the local scale. This subsurface groundwater circulation is evidence that the local topography plays a role at the local scale. This fact is of vital importance in Bangladesh, where it might play an important role in groundwater contamination by As. The results of the steady state flow model suggest the existence of a local scale flow net and the directions of groundwater flow are given by flowlines pointing that the local flow is from the manmade features toward the low-lying (cultivation) areas. The average vertical flow velocity is compatible with the previously reported one, 3 m/a (Dowling et al. 2002). The simulated streamlines do affect the advection velocity of the plume of contaminant laterally and vertically to a high extent. Whether these differences are large enough to alter sufficiently the conclusions of a contaminant risk

assessment has to be judged for each area individually. In fact, this will eventually depend on the precision of the other available hydraulic parameters of the aquifer model.

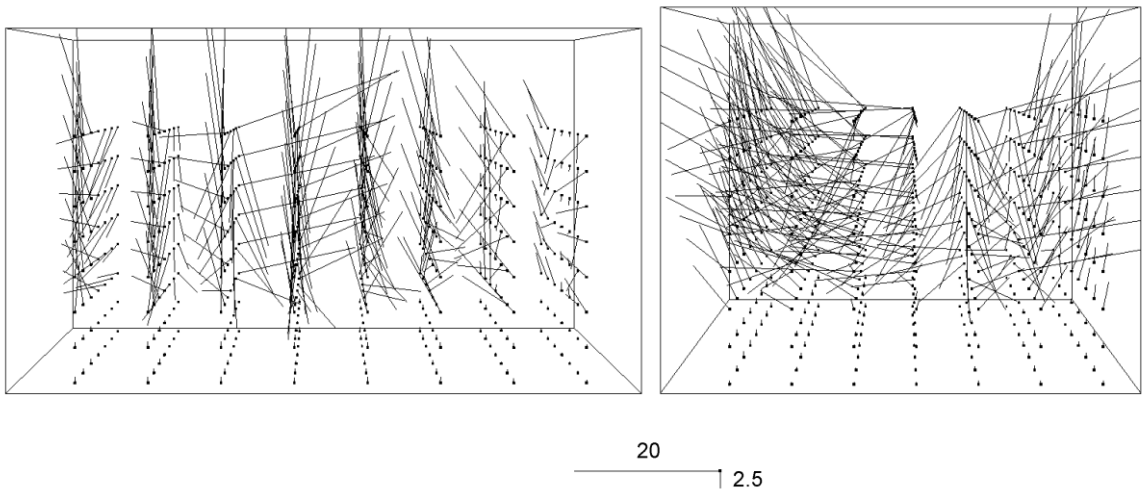

Figure 10: Flow vectors calculated by PHAST shown as a base point with a line indicating velocity and direction (left: side view, right: front view)

The simulated flow net could play the role of a transporting and distributing mechanism to distribute the contaminant upward and sideward in the underground farther from the origin. Also, this local circulation might leave behind at some depths stagnant zones, which could be a reasonable explanation for the reported juxtaposition of the old and recent groundwater ages at the same depth. With regard to As, this local scale flow net might be responsible for the patchy nature of As contamination reported in different studies (McArthur et al. 2004; Zheng et al. 2004; Zheng et al. 2005; Anawar et al. 2011).

Consequently, topography modification and pumping affect groundwater flow paths, which might induce changes in the underground e.g., shorten the residence time of groundwater and groundwater chemistry. Such changes can be responsible for stimulating microbial reactions that target the solid phase and destabilize sedimentary OC (Neumann et al. 2014).

5. CONCLUSIONS

Despite the limited amount of data and number of sample locations in this study, which may not be sufficient to understand the processes operating at the local scale (vertically and laterally), different concluding remarks could be drawn.

The hydrostratigraphic model has shown that silty-clay aquitard formations can neither have a uniform thickness nor occur at a uniform depth in the shallow aquifer, at least in the region of

interest. The anisotropy which might be induced by these irregularly distributed units beside the distinct continuous silt/clay layer (laterite surface) are important for the security of the deep groundwater. The second aquifer (> 100 mbgl) seems, at least in the studied scale, isolated to some extent from the upper shallow aquifer, which lessens the possibility of downward migration of arsenic/carbon-loaded groundwater. Thus, the reported arsenic, > 10 µg/L, in groundwater from the deep aquifer must have been released due to in-situ input of organic carbon. Thus, future studies regarding the arsenic problem in groundwater in Bangladesh should concentrate on the role of aquitards, whose spatial distribution affects the development of any hydrogeology-based mitigation scheme.

Highly populated deltas and floodplains are arsenic-affected areas (Winkel et al. 2008; Syvitski et al. 2009). The manmade changes induced by people in such areas by sediment mining for changing the natural landscape (beside other anthropogenic factors), might alter natural hydrological processes and groundwater flow paths. This is of vital importance for the sake of forecasting where arsenic exists, determining its future evolution, and implementing mitigation strategies. The results of the flow simulation showed that small anthropogenic perturbations (e.g., earth cutting to fill/raise land) are responsible for altering the subsurface flow regime and consequently the subsurface spatial distribution of contaminations. Such alterations in flow should be judiciously planned prior to major alterations in the landscape or groundwater extraction. Thus, arsenic-low wells may turn out to be contaminated after hydraulic flow perturbation; it is therefore important that safe wells be periodically re-tested for arsenic, especially after the onset of intensive irrigation pumping and large-scale excavation projects.

The idea that deeper irrigational pumping might spread arsenic to previously uncontaminated deep aquifers seems not to be correct in the light of the available data. The shallow and deep groundwaters appear to be isolated, and possible recharging of the deep aquifer from the eastern margin might lessen the problem of quantitative sustainability.

6. ACKNOWLEDGMENT

The authors are grateful to Dr. Mohammad A. Hoque and the Department of Public Health Engineering (DPHE) Bangladesh for providing the well log data.

7. REFERENCES

Acharyya S, Lahiri K, Raymahashay S, B. C., Bhowmik, A. (2000) Arsenic toxicity of groundwater in parts of the Bengal basin in India and Bangladesh: the role of Quaternary stratigraphy and Holocene sea-level fluctuation. Environmental Geology, 39(10), 1127–1137.

Aggarwal PK, Basu AR, Poreda RJ, Kulkarni KM, Froehlich K, Tarafdar SA, Ali M, Ahmed N, Hussain A, Rahman M, Ahmed SR (2000) A Report on Isotope Hydrology of Groundwater in Bangladesh: Implications for Characterization and Mitigation of Arsenic in Groundwater.

Aguilar L, Thibodeaux LJ (2005) Kinetics of peat soil dissolved organic carbon release from bed sediment to water. Part 1. Laboratory simulation. Chemosphere 58(10):1309–1318.

Ahmed MJ, Haque MR, Rahman MM (2010) Physicochemical Assessment of Surface and Groundwater Resources of Noakhali Region of Bangladesh. International Journal of Chemical and Environmental Engineering 1(1):47–55.

Akai J, Kanekiyo A, Hishida N, Ogawa M, Naganuma T, Fukuhara H, Anawar HN (2008) Biogeochemical characterization of bacterial assemblages in relation to release of arsenic from South East Asia (Bangladesh) sediments. Applied Geochemistry 23(11):3177–3186.

Al Lawati WM, Rizoulis A, Eiche E, Boothman C, Polya DA, Lloyd JR, Berg M, Vasquez-Aguilar P, van Dongen BE (2012) Characterisation of organic matter and microbial communities in contrasting arsenic-rich Holocene and arsenic-poor Pleistocene aquifers, Red River Delta, Vietnam. Applied Geochemistry 27(1):315–325.

Anawar HM, Akai J, Mihaljevič M, Sikder AM, Ahmed G, Tareq SM, Rahman MM (2011) Arsenic Contamination in Groundwater of Bangladesh: Perspectives on Geochemical, Microbial and Anthropogenic Issues. Water 3(4):1050–1076.

Argos M, Kalra T, Rathouz PJ, Chen Y, Pierce B, Parvez F, Islam T, Ahmed A, Rakibuz-Zaman M, Hasan R, Sarwar G, Slavkovich V, van Geen A, Graziano J, Ahsan H (2010) Arsenic exposure from drinking water, and all-cause and chronic-disease mortalities in Bangladesh (HEALS): a prospective cohort study. The Lancet 376(9737):252–258.

Aziz Z, van Geen A, Stute M, Versteeg R, Horneman A, Zheng Y, Goodbred S, Steckler M, Weinman B, Gavrieli I, Hoque MA, Shamsudduha M, Ahmed KM (2008) Impact of local

recharge on arsenic concentrations in shallow aquifers inferred from the electromagnetic conductivity of soils in Araihazar, Bangladesh. Water Resources Research 44(7):1–15.

Biester H, Keppler F, Putschew A, Martinez-Cortizas A, Petri M (2004) Halogen Retention, Organohalogens, and the Role of Organic Matter Decomposition on Halogen Enrichment in Two Chilean Peat Bogs. Environmental Science & Technology 38(7):1984–1991.

Biester H, Selimović D, Hemmerich S, Petri M (2006) Halogens in pore water of peat bogs – the role of peat decomposition and dissolved organic matter. Biogeosciences 3(1):53–64.

Biswas A, Bhattacharya P, Mukherjee A, Nath B, Alexanderson H, Kundu AK, Chatterjee D, Jacks G (2014) Shallow hydrostratigraphy in an arsenic affected region of Bengal Basin: Implication for targeting safe aquifers for drinking water supply. Science of The Total Environment 485–486(0):12–22.

Bundschuh J, Litter M, Bhattacharya P (2010) Targeting arsenic-safe aquifers for drinking water supplies. Environmental Geochemistry and Health 32(4):307–315.

Burgess WG, Burren M, Perrin J, Ahmed KM (2002) Constraints on sustainable development of arsenic-bearing aquifers in southern Bangladesh. Part 1: A conceptual model of arsenic in the aquifer. Geological Society Special Publication. Department of Geological Sciences, University College London, Gower Street, London WC1E 6BT, United Kingdom.

Burgess WG, Hoque MA, Michael HA, Voss CI, Breit GN, Ahmed KM (2010) Vulnerability of deep groundwater in the Bengal Aquifer System to contamination by arsenic. Nature Geoscience 3(2):83–87.

Cark I, Fritz P (1997) Environmental Isotopes in Hydrogeology. New York: Lewis Publishers.

Chakraborti D, Das B, Rahman MM, Chowdhury UK, Biswas B, Goswami AB, Nayak B, Pal A, Sengupta MK, Ahamed S, Hossain A, Basu G, Roychowdhury T, Das D (2009) Status of groundwater arsenic contamination in the state of West Bengal, India: A 20-year study report. Molecular Nutrition & Food Research 53(5):542–551.

Chen G, Auerswald K, Schnyder H (2016) 2H and 18O depletion of water close to organic surfaces. Biogeosciences 13(10):3175–3186.

Cheng Z, van Geen A, Seddique AA, Ahmed KM (2005) Limited Temporal Variability of

Arsenic Concentrations in 20 Wells Monitored for 3 Years in Araihazar, Bangladesh. Environmental Science & Technology 39(13):4759–4766.

Chowdhury UK, Biswas BK, Chowdhury TR, Samanta G, Mandal BK, Basu GC, Chanda CR, Lodh D, Saha KC, Mukherjee SK, Roy S, Kabir S, Quamruzzaman Q, Chakraborti D (2000) Groundwater arsenic contamination in Bangladesh and West Bengal, India. Environmental Health Perspectives 108(5):393–397.

Datta S, Neal AW, Mohajerin TJ, Ocheltree T, Rosenheim BE, White CD, Johannesson KH (2011) Perennial ponds are not an important source of water or dissolved organic matter to groundwaters with high arsenic concentrations in West Bengal, India. Geophysical Research Letters 38(20):1–5.

Davis SN, Thompson GM, Bentley HW, Stiles G (1980) Ground-Water Tracers — A Short Review. Ground Water 18(1):14–23.

Davis SN, Whittemore DO, Fabryka-Martin J (1998) Uses of Chloride/Bromide Ratios in Studies of Potable Water. Ground Water 36(2):338–350.

Desbarats AJ, Koenig CEM, Pal T, Mukherjee PK, Beckie RD (2014) Groundwater flow dynamics and arsenic source characterization in an aquifer system of West Bengal, India. Water Resources Research 50(6):4974–5002.

Dhar RK, Zheng Y, Stute M, van Geen A, Cheng Z, Shanewaz M, Shamsudduha M, Hoque MA, Rahman MW, Ahmed KM (2008) Temporal variability of groundwater chemistry in shallow and deep aquifers of Araihazar, Bangladesh. Journal of Contaminant Hydrology 99(1–4):97–111.

Dowling CB, Poreda RJ, Basu AR, Peters SL, Aggarwal PK (2002) Geochemical study of arsenic release mechanisms in the Bengal Basin groundwater. Water Resources Research 38(9):1173.

Drake H, Astrom ME, Heim C, Broman C, Astrom J, Whitehouse M, Ivarsson M, Siljestrom S, Sjovall P (2015) Extreme 13C depletion of carbonates formed during oxidation of biogenic methane in fractured granite. Nature Communications 6(7020):1–9.

Eiche E, Neumann T, Berg M, Weinman B, van Geen A, Norra S, Berner Z, Trang PTK, Viet

PH, Stüben D (2008) Geochemical processes underlying a sharp contrast in groundwater arsenic concentrations in a village on the Red River delta, Vietnam. Applied Geochemistry 23(11):3143–3154.

Fontaine S, Barot S, Barre P, Bdioui N, Mary B, Rumpel C (2007) Stability of organic carbon in deep soil layers controlled by fresh carbon supply. Nature 450(7167):277–280.

van Geen A, Ahmed KM, Akita Y, Alam MJ, Culligan PJ, Emch M, Escamilla V, Feighery J, Ferguson AS, Knappett P, Layton AC, Mailloux BJ, McKay LD, Mey JL, Serre ML, Streatfield PK, Wu J, Yunus M (2011) Fecal Contamination of Shallow Tubewells in Bangladesh Inversely Related to Arsenic. Environmental Science & Technology 45(4):1199–1205.

van Geen A, Zheng Y, Goodbred S, Horneman A, Aziz Z, Cheng Z, Stute M, Mailloux B, Weinman B, Hoque MA, Seddique AA, Hossain MS, Chowdhury SH, Ahmed KM (2008) Flushing History as a Hydrogeological Control on the Regional Distribution of Arsenic in Shallow Groundwater of the Bengal Basin. Environmental Science & Technology 42(7):2283–2288.

van Geen A, Zheng Y, Versteeg R, Stute M, Horneman A, Dhar R, Steckler M, Gelman A, Small C, Ahsan H, Graziano JH, Hussain I, Ahmed KM (2003) Spatial variability of arsenic in 6000 tube wells in a 25 km2 area of Bangladesh. Water Resources Research 39(5):1140.

Ghosh D, Routh J, Dario M, Bhadury P (2015) Elemental and biomarker characteristics in a Pleistocene aquifer vulnerable to arsenic contamination in the Bengal Delta Plain, India. Applied Geochemistry 61:87–98.

Goodbred JSL, Kuehl SA (2000) The significance of large sediment supply, active tectonism, and eustasy on margin sequence development: Late Quaternary stratigraphy and evolution of the Ganges–Brahmaputra delta. Sedimentary Geology 133(3–4):227–248.

Han LF, Niel Plummer L, Aggarwal P (2014) The curved 14C vs. δ13C relationship in dissolved inorganic carbon: A useful tool for groundwater age- and geochemical interpretations. Chemical Geology 387:111–125.

Harvey CF, Ashfaque KN, Yu W, Badruzzaman ABM, Ali MA, Oates PM, Michael HA, Neumann RB, Beckie R, Islam S, Ahmed MF (2006) Groundwater dynamics and arsenic

contamination in Bangladesh. Chemical Geology 228(1–3):112–136.

Harvey CF, Swartz CH, Badruzzaman ABM, Keon-Blute N, Yu W, Ali MA, Jay J, Beckie R, Niedan V, Brabander D, Oates PM, Ashfaque KN, Islam S, Hemond HF, Ahmed MF (2002) Arsenic Mobility and Groundwater Extraction in Bangladesh. Science 298(5598):1602–1606.

Hoque MA, Burgess WG (2012) 14C dating of deep groundwater in the Bengal Aquifer System, Bangladesh: Implications for aquifer anisotropy, recharge sources and sustainability. Journal of Hydrology 444–445:209–220.

Hoque MA, McArthur JM, Sikdar PK (2012) The palaeosol model of arsenic pollution of groundwater tested along a 32 km traverse across West Bengal, India. Science of The Total Environment 431:157–165.

Hoque MA, McArthur JM, Sikdar PK (2014) Sources of low-arsenic groundwater in the Bengal Basin: investigating the influence of the last glacial maximum palaeosol using a 115-km traverse across Bangladesh. Hydrogeology Journal 22(7):1535–1547.

Hoque M, Khan A, Shamsudduha M, Hossain M, Islam T, Chowdhury S (2009) Near surface lithology and spatial variation of arsenic in the shallow groundwater: southeastern Bangladesh. Environmental Geology 56(8):1687–1695.

Horneman A, van Geen A, Kent DV, Mathe PE, Zheng Y, Dhar RK, O'Connell S, Hoque MA, Aziz Z, Shamsudduha M, Seddique AA, Ahmed KM (2004) Decoupling of As and Fe release to Bangladesh groundwater under reducing conditions. Part I: Evidence from sediment profiles. Geochimica et Cosmochimica Acta 68(17):3459–3473.

Hossain MF (2006) Arsenic contamination in Bangladesh—An overview. Agriculture, Ecosystems & Environment 113(1–4):1–16.

Hossain MM, Piantanakulchai M (2013) Groundwater arsenic contamination risk prediction using GIS and classification tree method. Engineering Geology 156:37–45.

Islam FS, Gault AG, Boothman C, Polya DA, Charnock JM, Chatterjee D, Lloyd JR (2004) Role of metal-reducing bacteria in arsenic release from Bengal delta sediments. Nature 430(6995):68–71.

Kabata-Pendias A (2001) Trace elements in soils and plants (3rd ed.). CRC Press LLC.

Kanoua W, Merkel B (2015) Modification of a digital elevation model (DEM) in a flat topographic area with respect to manmade features. Geosciences Journal 20(1):101–115.

Kanoua W, Merkel B (2017) Hydrochemical evolution and arsenic release in shallow aquifer in the Titas Upazila, Eastern Bangladesh. Arabian Journal of Geosciences 10(13):290–304.

Kelleher BP, Simpson AJ (2006) Humic Substances in Soils: Are They Really Chemically Distinct? Environmental Science & Technology 40(15):4605–4611.

Khan TA, Rahman A, Ali I, Khan J, Alam SD (2016) Assessing spatial variations of groundwater arsenic with surface elevation, slope and water-table using geospatial techniques in Ballia district, India. Modeling Earth Systems and Environment 2(83):1–12.

Klump S, Kipfer R, Cirpka OA, Harvey CF, Brennwald MS, Ashfaque KN, Badruzzaman ABM, Hug SJ, Imboden DM (2006) Groundwater Dynamics and Arsenic Mobilization in Bangladesh Assessed Using Noble Gases and Tritium. Environmental Science & Technology 40(1):243–250.

Kulkarni HV, Mladenov N, Johannesson KH, Datta S (2016) Contrasting dissolved organic matter quality in groundwater in Holocene and Pleistocene aquifers and implications for influencing arsenic mobility. Applied Geochemistry 77:194-205.

Leber J, Rahman MM, Ahmed KM, Mailloux B, van Geen A (2011) Contrasting Influence of Geology on E. coli and Arsenic in Aquifers of Bangladesh. Ground Water 49(1):111–123.

Lehmann J, Solomon D, Kinyangi J, Dathe L, Wirick S, Jacobsen C (2008) Spatial complexity of soil organic matter forms at nanometre scales. Nature Geosci. 1(4):238–242.

Mailloux BJ, Trembath-Reichert E, Cheung J, Watson M, Stute M, Freyer GA, Ferguson AS, Ahmed KM, Alam MJ, Buchholz BA, Thomas J, Layton AC, Zheng Y, Bostick BC, van Geen A (2013) Advection of surface-derived organic carbon fuels microbial reduction in Bangladesh groundwater. Proceedings of the National Academy of Sciences 110(14):5331–5335.

Maitra MK, Ashraful Islam M, Al Mamun M (2014). Thickness Distribution and Quality Assessment of Gopalganj-Madaripur Peat Deposits : A Case Study of Potential Economic Opportunities in Mid-Eastern. Earth & Environmental Sciences, 5(9), 943–955.

Majumdar PK, Ghosh NC, Chakravorty B (2002) Analysis of arsenic-contaminated groundwater domain in the Nadia district of West Bengal (India). Hydrological Sciences Journal 47(S1):55–66.

Majumder RK, Shimada J, Taniguchi M (2013) Groundwater flow systems in the Bengal Delta, Bangladesh, inferred from subsurface temperature readings. Songklanakarin Journal of Science and Technology 35(1):99–106.

McArthur JM, Banerjee DM, Hudson-Edwards KA, Mishra R, Purohit R, Ravenscroft P, Cronin A, Howarth RJ, Chatterjee A, Talukder T, Lowry D, Houghton S, Chadha DK (2004) Natural organic matter in sedimentary basins and its relation to arsenic in anoxic ground water: the example of West Bengal and its worldwide implications. Applied Geochemistry 19(8):1255–1293.

McArthur JM, Ghosal U, Sikdar PK, Ball JD (2016) Arsenic in Groundwater: The Deep Late Pleistocene Aquifers of the Western Bengal Basin. Environmental Science & Technology 50(7):3469–3476.

McArthur JM, Nath B, Banerjee DM, Purohit R, Grassineau N (2011) Palaeosol Control on Groundwater Flow and Pollutant Distribution: The Example of Arsenic. Environmental Science & Technology 45(4):1376–1383.

McArthur JM, Ravenscroft P, Banerjee DM, Milsom J, Hudson-Edwards KA, Sengupta S, Bristow C, Sarkar A, Tonkin S, Purohit R (2008) How paleosols influence groundwater flow and arsenic pollution: A model from the Bengal Basin and its worldwide implication. Water Resources Research 44(11):1–30.

McArthur JM, Ravenscroft P, Safiulla S, Thirlwall MF (2001) Arsenic in groundwater: Testing pollution mechanisms for sedimentary aquifers in Bangladesh. Water Resources Research 37(1):109–117.

McArthur JM, Sikdar PK, Hoque MA, Ghosal U (2012) Waste-water impacts on groundwater: Cl/Br ratios and implications for arsenic pollution of groundwater in the Bengal Basin and Red River Basin, Vietnam. Science of The Total Environment 437:390–402.

McMahon PB (2001) Aquifer/aquitard interfaces: Mixing zones that enhance biogeochemical reactions. Hydrogeology Journal 9(1):34–43.

McNichol AP, Osborne EA, Gagnon AR, Fry B, Jones GA (1994) TIC, TOC, DIC, DOC, PIC, POC — unique aspects in the preparation of oceanographic samples for 14C-AMS. Nuclear Instruments and Methods in Physics Research Section B: Beam Interactions with Materials and Atoms 92(1):162–165.

Michael HA, Voss CI (2008) Evaluation of the sustainability of deep groundwater as an arsenic-safe resource in the Bengal Basin. Proceedings of the National Academy of Sciences of the United States of America 105(25):8531–8536.

Michael HA, Voss CI (2009) Estimation of regional-scale groundwater flow properties in the Bengal Basin of India and Bangladesh. Hydrogeology Journal 17(6):1329–1346.

Mihajlov I, Stute M, Schlosser P, Mailloux BJ, Zheng Y, Choudhury I, Ahmed KM, van Geen A (2016) Recharge of low-arsenic aquifers tapped by community wells in Araihazar, Bangladesh, inferred from environmental isotopes. Water Resources Research 52(5):3324–3349.

Mladenov N, Zheng Y, Miller MP, Nemergut DR, Legg T, Simone B, Hageman C, Rahman MM, Ahmed KM, McKnight DM (2010) Dissolved Organic Matter Sources and Consequences for Iron and Arsenic Mobilization in Bangladesh Aquifers. Environmental Science & Technology 44(1):123–128.

Mladenov N, Zheng Y, Simone B, Bilinski TM, McKnight DM, Nemergut D, Radloff KA, Rahman MM, Ahmed KM (2015) Dissolved Organic Matter Quality in a Shallow Aquifer of Bangladesh: Implications for Arsenic Mobility. Environmental Science & Technology 49(18):10815–10824.

Mukherjee A, Fryar A, Howell P (2007) Regional hydrostratigraphy and groundwater flow modeling in the arsenic-affected areas of the western Bengal basin, West Bengal, India. Hydrogeology Journal 15(7):1397–1418.

Neumann RB, Ashfaque KN, Badruzzaman ABM, Ashraf Ali M, Shoemaker JK, Harvey CF (2010) Anthropogenic influences on groundwater arsenic concentrations in Bangladesh. Nature Geosci. 3(1):46–52.

Neumann RB, Pracht LE, Polizzotto ML, Badruzzaman ABM, Ali MA (2014) Biodegradable Organic Carbon in Sediments of an Arsenic-Contaminated Aquifer in Bangladesh.

Environmental Science & Technology Letters 1(4):221–225.

Nickson RT, McArthur JM, Ravenscroft P, Burgess WG, Ahmed KM (2000) Mechanism of arsenic release to groundwater, Bangladesh and West Bengal. Applied Geochemistry 15(4):403–413.

Planer-Friedrich B, Härtig C, Lissner H, Steinborn J, Süß E, Qumrul Hassan M, Zahid A, Alam M, Merkel B (2012) Organic carbon mobilization in a Bangladesh aquifer explained by seasonal monsoon-driven storativity changes. Applied Geochemistry 27(12):2324–2334.

Polizzotto ML, Harvey CF, Sutton SR, Fendorf S (2005) Processes conducive to the release and transport of arsenic into aquifers of Bangladesh. In Proceedinqs of the National Academy of Sciences of the United States of America 102(52):18819–18823.

Postma D, Larsen F, Minh Hue NT, Duc MT, Viet PH, Nhan PQ, Jessen S (2007) Arsenic in groundwater of the Red River floodplain, Vietnam: Controlling geochemical processes and reactive transport modeling. Geochimica et Cosmochimica Acta 71(21):5054–5071.

Radloff KA, Zheng Y, Michael HA, Stute M, Bostick BC, Mihajlov I, Bounds M, Huq MR, Choudhury I, Rahman MW, Schlosser P, Ahmed KM, van Geen A (2011) Arsenic migration to deep groundwater in Bangladesh influenced by adsorption and water demand. Nature Geosci. 4(11):793–798.

Radloff KA, Zheng Y, Stute M, Weinman B, Bostick B, Mihajlov I, Bounds M, Rahman MM, Huq MR, Ahmed KM, Schlosser P, van Geen A (2017) Reversible adsorption and flushing of arsenic in a shallow, Holocene aquifer of Bangladesh. Applied Geochemistry 17:142-157.

Ravenscroft P, Burgess W, Ahmed K, Burren M, Perrin J (2005) Arsenic in groundwater of the Bengal Basin, Bangladesh: Distribution, field relations, and hydrogeological setting. Hydrogeology Journal 13(5–6):727–751.

Ravenscroft P, McArthur J, Hoque BA (2001) Geochemical and Palaeohydrological Controls on Pollution of Groundwater by Arsenic. In Chappell WR, Abernathy CO, Calderon R (Eds.), Arsenic Exposure and Health Effects IV (pp. 53–77). Oxford: Elsevier Science Ltd.

Rowland HAL, Polya DA, Lloyd JR, Pancost RD (2006) Characterisation of organic matter in a shallow, reducing, arsenic-rich aquifer, West Bengal. Organic Geochemistry 37(9):1101–

1114.

Roychowdhury T (2010) Groundwater arsenic contamination in one of the 107 arsenic-affected blocks in West Bengal, India: Status, distribution, health effects and factors responsible for arsenic poisoning. International Journal of Hygiene and Environmental Health 213(6):414–427.

Sarkar A, Sengupta S, McArthur JM, Ravenscroft P, Bera MK, Bhushan R, Samanta A, Agrawal S (2009) Evolution of Ganges–Brahmaputra western delta plain: Clues from sedimentology and carbon isotopes. Quaternary Science Reviews 28(25–26):2564–2581.

Saunders JA, Lee MK, Shamsudduha M, Dhakal P, Uddin A, Chowdury MT, Ahmed KM (2008) Geochemistry and mineralogy of arsenic in (natural) anaerobic groundwaters. Applied Geochemistry 23(11):3205–3214.

Savarimuthu X, Hira-Smith MM, Yuan Y, von Ehrenstein OS, Das S, Ghosh N, Mazumder DNG, Smith AH (2006) Seasonal Variation of Arsenic Concentrations in Tubewells in West Bengal, India. J Health Popul Nutr. 24(3):277–281.

Schmidt MWI, Torn MS, Abiven S, Dittmar T, Guggenberger G, Janssens IA, Kleber M, Kogel-Knabner I, Lehmann J, Manning DAC, Nannipieri P, Rasse DP, Weiner S, Trumbore SE (2011) Persistence of soil organic matter as an ecosystem property. Nature 478(7367):49–56.

Schweizer M, Fear J, Cadisch G (1999) Isotopic (13C) fractionation during plant residue decomposition and its implications for soil organic matter studies. Rapid Communications in Mass Spectrometry 13(13):1284–1290.

Sengupta S, McArthur JM, Sarkar A, Leng MJ, Ravenscroft P, Howarth RJ, Banerjee DM (2008) Do Ponds Cause Arsenic-Pollution of Groundwater in the Bengal Basin? An Answer from West Bengal. Environmental Science & Technology 42(14):5156–5164.

Shamsudduha M (2007) Spatial Variability and Prediction Modeling of Groundwater Arsenic Distributions in the Shallowest Alluvial Aquifers in Bangladesh. Journal of Spatial Hydrology 7(2):33–46.

Shamsudduha M, Marzen LJ, Uddin A, Lee M.K, Saunders JA (2009) Spatial relationship of

groundwater arsenic distribution with regional topography and water-table fluctuations in the shallow aquifers in Bangladesh. Environmental Geology 57(7):1521–1535.

Singh SK, Trivedi JR, Pande K, Ramesh R, Krishnaswami S (1998) Chemical and Strontium, Oxygen, and Carbon Isotopic Compositions of Carbonates from the Lesser Himalaya: Implications to the Strontium Isotope Composition of the Source Waters of the Ganga, Ghaghara, and the Indus Rivers. Geochimica et Cosmochimica Acta 62(5):743–755.

Singh TP, Gupta VK (2008) Arsenic intoxication presenting as peripheral neuropathy and dermatological disorder. Journal, Indian Academy of Clinical Medicine 9(2):150–152.

Smith AH, Lingas EO, Rahman M (2000) Contamination of drinking-water by arsenic in Bangladesh: A public health emergency. Bulletin of the World Health Organization 78(9):1093–1103.

Stute M, Zheng Y, Schlosser P, Horneman A, Dhar RK, Datta S, Hoque MA, Seddique AA, Shamsudduha M, Ahmed KM, van Geen A (2007) Hydrological control of As concentrations in Bangladesh groundwater. Water Resources Research 43(9):1–11.

Sultana F (2007) Sustainable Water Supply: Rainwater Harvesting for Multistoried Residential Apartments in Dhaka, Bangladesh. Texas A&M University.

Swartz CH, Blute NK, Badruzzman B, Ali A, Brabander D, Jay J, Besancon J, Islam S, Hemond HF, Harvey CF (2004) Mobility of arsenic in a Bangladesh aquifer: Inferences from geochemical profiles, leaching data, and mineralogical characterization. Geochimica et Cosmochimica Acta 68(22):4539–4557.

Syvitski JPM, Kettner AJ, Overeem I, Hutton EWH, Hannon MT, Brakenridge GR, Day J, Vörösmarty C, Saito Y, Giosan L, Nicholls RJ (2009) Sinking deltas due to human activities. Nature Geoscience 2(10):681–686.

Tareq SM, Maruo M, Ohta K (2013) Characteristics and role of groundwater dissolved organic matter on arsenic mobilization and poisoning in Bangladesh. Physics and Chemistry of the Earth, Parts A/B/C, 58–60, 77–84.

Tathagata G, Rolee K (2011) Spatio-Temporal Pattern of Groundwater Arsenic Concentration in Thick Unconfined Aquifer of Murshidabad District, West Bengal, India. Universal Journal

of Environmental Research and Technology 1(3):311–319.

Thurman EM (1985) Organic Geochemistry of Natural Waters (1st ed.). Dordrecht: Springer Netherlands.

Tóth J (2009) Gravitational Systems of Groundwater Flow: Theory, Evaluation, Utilization. Cambridge University Press.

Tufano KJ, Fendorf S (2008) Confounding Impacts of Iron Reduction on Arsenic Retention. Environmental Science & Technology 42(13):4777–4783.

Uddin MS, Kurosawa K (2014) Effects of peat and water quality parameters on groundwater arsenic contamination in Bangladesh. Water and Environment Journal 28(2):165–172.

Umitsu M (1993) Late quaternary sedimentary environments and landforms in the Ganges Delta. Sedimentary Geology 83(3–4):177–186.

Wang S, Mulligan CN (2006) Effect of natural organic matter on arsenic release from soils and sediments into groundwater. Environmental Geochemistry and Health 28(3):197–214.

Weinman B, Goodbred SL, Zheng Y, Aziz Z, Steckler M, van Geen A, Singhvi AK, Nagar YC (2008) Contributions of floodplain stratigraphy and evolution to the spatial patterns of groundwater arsenic in Araihazar, Bangladesh. Geological Society of America Bulletin 120(11–12):1567–1580.

Whaley-Martin KJ, Mailloux BJ, van Geen A, Bostick BC, Silvern RF, Kim C, Ahmed KM, Choudhury I, Slater GF (2016) Stimulation of Microbially Mediated Arsenic Release in Bangladesh Aquifers by Young Carbon Indicated by Radiocarbon Analysis of Sedimentary Bacterial Lipids. Environmental Science & Technology 50(14):7353–7363.

Whiticar MJ (1999) Carbon and hydrogen isotope systematics of bacterial formation and oxidation of methane. Chemical Geology 161(1–3):291–314.

Winkel L, Berg M, Amini M, Hug SJ, Annette Johnson C (2008) Predicting groundwater arsenic contamination in Southeast Asia from surface parameters. Nature Geosci. 1(8):536–542.

Wynn JG (2007) Carbon isotope fractionation during decomposition of organic matter in soils

and paleosols: Implications for paleoecological interpretations of paleosols. Palaeogeography, Palaeoclimatology, Palaeoecology 251(3–4):437–448.

Zheng Y, Stute M, van Geen A, Gavrieli I, Dhar R, Simpson HJ, Schlosser P, Ahmed KM (2004) Redox control of arsenic mobilization in Bangladesh groundwater. Applied Geochemistry 19(2):201–214.

Zheng Y, van Geen A, Stute M, Dhar R, Mo Z, Cheng Z, Horneman A, Gavrieli I, Simpson HJ, Versteeg R, Steckler M, Grazioli-Venier A, Goodbred S, Shahnewaz M, Shamsudduha M, Hoque MA, Ahmed K (2005) Geochemical and hydrogeological contrasts between shallow and deeper aquifers in two villages of Araihazar, Bangladesh: Implications for deeper aquifers as drinking water sources. Geochimica et Cosmochimica Acta 69(22):5203–5218.

Zijl W (1999) Scale aspects of groundwater flow and transport systems. Hydrogeology Journal 7(1):139–150.

Zobrist J, Davis JA, Oremland RS (2000) Mobilization of Arsenite by Dissimilatory Reduction of Adsorbed Arsenate. Environ. Sci. Technol. 34(22):4747–4753.

Estimating actual Evapotranspiration in Hanoi with SEBAL

Hung V. Vu *)
Hydrogeology Department, Institute for Geologie, TU Bergakademie Freiberg, 09599 Freiberg, Germany.
hungvu2003@gmail.com
Department of Hydrogeology, Faculty of Geology, Hanoi University of Mining and Geology, 10000 Hanoi, Vietnam.

Broder J. Merkel
Hydrogeology Department, Institute for Geologie, TU Bergakademie Freiberg, 09599 Freiberg, Germany

Abstract: Evapotranspiration (ET) is the most critical parameter in the hydrologic cycle with respect to determination. Several mathematical equations exist to estimate this value. Some of them are based on energy or water balances coupled with data from meteorological stations. In this work, the actual evapotranspiration (AE) in Hanoi area was estimated by means of the Surface Energy Balance Algorithm for Land (SEBAL) with four Landsat Thematic Mapper images (TM5). In addition, meteorological data from four weather stations from 1961 to 2010 was used. The spatial and temporal distribution of AE was visualized. Then, the estimated AE was compared with the potential evaporation (PE) calculated using the Penmann – Monteith equation and evaporation (Ep) measured with the pan class A. The means of AE range between 1.73 mm/d and 2.25 mm/d, which were calculated for February and May, respectively. The spatial and temporal distribution of AE was also compared with the land use vegetation cover map for 2007. Finally, using the evaporative fraction, the seasonal AE was interpolated for the entire area. The annual AE estimated by the SEBAL model is 751 mm accounting for 86% of PE and 82% of Ep.

Keywords: actual evapotranspiration, potential evaporation, Penmann – Monteith equation, Hanoi, SEBAL, Vietnam.

1. INTRODUCTION

Because water is a prerequisite for human life, it is understandable how difficult human life in semi-arid or arid areas can be because of water shortage. Despite being considered a city rich in water resources and tropical climate, Hanoi faces as well several water supply issues (Nguyen V. Lam et al., 2012) such as:

- Water pollution due to industrial development,
- Over-pumping of groundwater,
- Leakage of water from the water supply network in summer when water demands reach the highest peak, and
- Steady population growth and water demands increase.

Recently, the major amount of water for Hanoi is extracted from groundwater. Another source is surface water from the Hoa Binh Reservoir 50 km from Hanoi. The total amount of water that is being supplied is approximately 1,600,000 m^3/d (VUSTA, 2012). Although this is a very high amount, it is still hard to meet the actual demand during the summer season. This issue requires thorough planning regarding integrated water resources management in order to compensate the water shortage during summer. To handle the problem, it is necessary to have a better understanding and knowledge of the water balance with all input and output parameters. Among them, the actual evapotranspiration (AE) is probably one of the most critical parameters. It is difficult to determine precisely and can only be estimated. However, to the best of the authors' knowledge, there is not yet any sufficient study estimating this parameter in the area. Only educated guesses about the actual evaporation of the Hanoi area exist in the literature (Nguyen V. Lam et al., 2012) and unpublished reports. Based on an educated guess, is is supposed that ET could be accounted for around 80% potential evaporation, because Hanoi is mostly covered by lakes, ponds, streams, and a vast area of paddy rice.

ET is one of the six major components of the hydrological cycle. Up to 60 % of land precipitation returns to the atmosphere by land evapotranspiration (Oki; Kanae, 2006; Jung, Martin et al., 2010). ET is composed of two processes being surface evaporation and plant transpiration. ET is controlled by several factors such as temperature, humidity, wind speed, water availability, soil type, plant type, and morphology (Bastiaanssen, 1998a; Hoekstra, Shachak, 1999; Khalili et al., 2014). ET can be measured in the field for one spot, but it is difficult, if not impossible, to interpolate these spot values to a regional scale (Allen, 1998; Paron et al., 2014). Until now, there is no comprehensive study on the AE in Hanoi; only provisional values based on experience or theoretical knowledge is available (Nguyen V. Lam et al., 2012). This lack of information has strongly motivated the authors to determine a more accurate AE value for the Hanoi area.

Several methods based on the energy balance and water balance equation may be used to estimate the AE. Among them are the remote sensing based method of SEBAL (Bastiaanssen 1998a, 1998b, 2000) and the Mapping Evapotranspiration at High Resolution using Internalized Calibration (METRIC) (Allen et al., 2007a; Allen et al., 2007b) are two conventional procedures. Some other models are the Two Sources Energy Balance model (TSEB) (Kustas, Norman, 2000), the Surface Energy Balance System (SEBS) (Su, 2002), the Remote Sensing of Evapotranspiration (ReSET) (Elhaddad, Garcia, 2008), the Analytical Land Atmosphere Radiometer Model (ALARM) (Ayman A Suleiman et al., 2009), and the Simplified Surface Energy Balance Index (S-SEBI) (Roerink et al., 2000). A review for S-SEBI, SEBS, TSEB, METRIC, and SEBAL can be found in (Liou, and Kar, 2014). Based on the surface energy balance equation, these methods calculate all components of the energy balance and then estimate the energy available for evaporation as a residual value. Because the heat that absorbed to convert one kilogram of water to vapor is a constant value, AE can be calculated from the consumption of energy for converting water to water vapor.

Water balance methods are based on the water balance equation, which links the input and output components. AE can be evaluated if data on runoff, precipitation, condensation, infiltration, and percolation is available (Allen, 1998; Elizabeth A. H., and Robert E. C., 2013, Senay et al., 2011, 2011; Elizabeth A. H., and Robert E. C., 2013).

SEBAL model costs are low, but it is a complicated procedure. It is obliged to select „hot" and "cold" pixels in SEBAL model. In the „hot" pixels, the latent heat flux is assumed to be zero, so the ET based on equation (2) should be zero. In the cold pixels, the sensible heat flux is theorized to zero and surface temperature, and near-surface air temperatures are assumed to be similar to each other (Bastiaanssen, 2000). However, SEBAL does not work with images covered by cloud. In addition to, a specific regression model is used in SEBAL, which might not be suitable for any topography. There is a big difference between AE in mountainous and plain areas. Thus one has to separate mountainous and plain areas in the calculation.

SEBAL model has been tested for various climatic conditions, and thesresults are reasonable (Bastiaanssen et al., 2005). One big advantage is that SEBAL requires only minimum ground-based measurements. In this study SEBAL was applied to estimate the daily AE for Hanoi using four Landsat TM5 images. Subsequently, the spatial and temporal distribution of AE is obtained. Finally, AE was compared with Ep (evaporation measured at the pan class A at weather stations) and PE.

Based on data of temperature, wind speed, sunshine duration, and humidity at weather stations PE can be calculated by the equations of Blaney – Criddle, Thornthwaite, Hargreaves, Turc, and Penmann – Monteith (Wilm et al., 1944; Turc, 1961; Hargreaves, G.H. and Samani, Z.A, 1985; Allen, 1998; Jacobs, Satti, 2001; Senay et al., 2008; Bhaskar R. Nikam et al, 2014; Djaman et al., 2015). This leads to an estimated PE for the whole Red River Delta (including Chinese territory). Le et al., (2012) recommended the use of the Turc and Penmann – Monteith equations because th other equations only consider temperature or sunshine duration so that the estimated PE values are higher than the evaporation actually measured in pans class A at the weather stations. In this study, PE was estimated by the Penmann – Monteith equation included in the software CROPWAT (Allen 1998).

2. STUDY AREA

Hanoi is the capital of the Socialist Republic of Vietnam and located in the northern part of Vietnam within the Red River Plain. Its area is 3,324 km², and the metropolitan area ranges from $20^0$53' to $21^0$23'N latitude and from $105^0$44 to $106^0$02E longitude. There are two main types of terrains: the plain area and the mountainous area. The topography decreases gently from north to south and from west to east. The mountainous area covers around 5 % of the study area and is concentrated in the northern and western part. The highest peak with 1,281 meters above sea level (m.a.s.l) lies in the west. Agricultural areas cover most of the Hanoi Plain, and the mean elevation ranges from 5 to 15 m.a.s.l (highlighted with green color in the land use vegetation cover map in Figure 1). The Red River, the mainstream in North Vietnam, flows through the Red River delta from the northwest to the southeast. Some small rivers in Hanoi are Duong, Cau, Ca Lo, Day, Lu, Set, Nhue, To Lich, and Kim Nguu. The biggest lake in the city is West Lake.

Hanoi is characterized by a warm, humid subtropical climate. This is the typical climate of northern Vietnam with heavy rain during the monsoon season. It is hot and wet in summer, and cold and drier in winter. The average precipitation between 1961 and 2010 was around 1700 mm/year. Significant rainfall occurs from May to October, accounting for 84 % of annual precipitation. The precipitation peaks in July and August (the warmest months of the year) with nearly 300 mm/month (Figure 2).

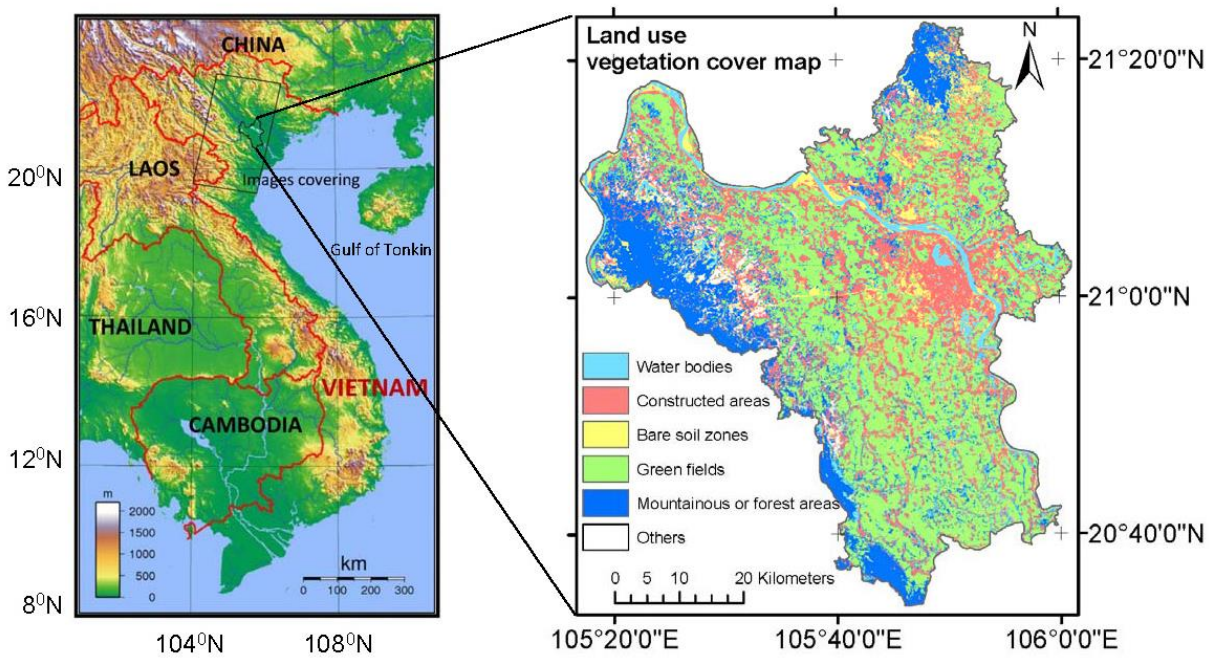

Figure. 1. The study area and the land use vegetation cover map from May 2007 (based on the Landsat TM5 image from May 8, 2007).

During the winter season, Hanoi receives less rainfall with around 25 mm/month corresponding to the lowest temperature. PE changes only slightly due to seasonal differences because the humidity is relatively high throughout the year. The average PE is about 73 mm/month with a total PE of nearly 900 mm/a accounting for about 50 % of precipitation (NCHMF, 1961-2010).

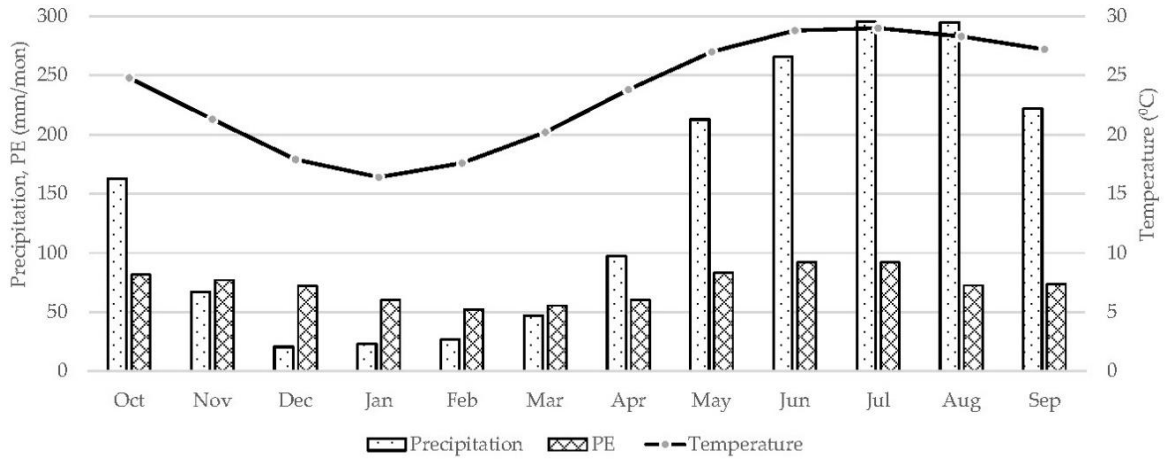

Figure. 2. Monthly averages of the meteorological parameters in Hanoi modified according to (NCHMF 1961-2010)

3. METHODOLOGY

AE calculation in SEBAL is based on the surface energy balance equation (Monteith, Unsworth, 1990; Bastiaanssen, 1998a, 2000; Allen et al., 2007b; Cuxart et al., 2015).

$$LE = R_n - H - G \quad (1)$$

where R_n is the net radiation (W/m^2), H is the sensible heat flux (W/m^2), G is the soil heat flux (W/m^2), and LE is latent heat flux (W/m^2). If all parameters on the right side of equation (1) are known, the latent heat flux can be calculated as a residual value for each cell. That value is then converted to the height of the water column undergoing ET based on the latent heat of vaporization (λ) and water density (ρ_w).

$$E_{inst} = \frac{LE}{\lambda \rho_w} \quad (2)$$

where E_{inst} is the instantaneous evapotranspiration.

The net radiation (R_n) is calculated according to equation (3).

$$R_n = (1 - \alpha)R_{S\_in} + R_{L\_in} - R_{L\_out} - (1 - \varepsilon_0)R_{L\_in} \quad (3)$$

where α is the surface albedo, R_{S_in} is the incoming shortwave radiation (W/m^2), R_{L_in} is the incoming longwave radiation (W/m^2), ε_0 is the surface emissivity, and R_{L_out} is the outgoing longwave radiation (W/m^2). All parameters used to calculate R_n can be found or estimated merely in the header file attached in image packages (Waters et al., 2002)

The soil heat flux (G) is the rate of heat storage in the soil and vegetation due to conduction. A common way to compute G is using equation (4) (Bastiaanssen, 2000) for calculating G/R_n.

$$G/R_n = T_s/\alpha(0.0038\alpha + 0.0074\alpha^2)(1 - 0.98NDVI^4) \quad (4)$$

where, R_n is the net radiation (W/m^2), T_s is the surface temperature (^0C), α is the surface albedo, and NDVI is the Normalized Difference Vegetation Index. Finally, G is calculated by multiplying G/R_n by R_n.

The sensible heat flux (H) is the process where heat is transferred from the earth's surface to the atmosphere by conduction and convection. The classical computation of H is described in (Farah, Bastiaanssen, 2001; Waters et al., 2002) as shown in equation (5).

$$H = \frac{\rho c_p dT}{r_{ah}} \quad (5)$$

where ρ is the air density (kg/m), c_p is the air-specific heat capacity (at constant pressure), 1004 J/(kg·K), dT is the temperature difference between 0.1 m, and 2.0 m above ground, respectively, and r_{ah} is the aerodynamic resistance to heat transport (s/m).

The sensible heat flux (H) is considered as a function of the temperature difference, surface roughness and wind speed (Sobrino 2002). With the data from the meteorological stations, dT and r_{ah} can be estimated. In the SEBAL the relationship between the temperature difference (dT) and the surface temperature (T_s) is assumed to be linear (Bastiaanssen, 1998a; Di Long et al., 2011; Waters et al., 2002).

$$dT = aT_s + b \quad (6)$$

where a and b are the correlation coefficients between dT and T_s.

To estimate a and b in equation (6), the „hot" and "cold" pixels (or anchor pixels) should be used. The „hot" and "cold" pixels should be in the area of interest. The "cold" pixel is selected to meet the requirements of a wet pixel covering by vegetation. The „hot" one is selected as a dry and bare agricultural field, where ET is assumed to be zero (Waters et al., 2000). Both of these "anchor" pixels should be located in large and homogeneous areas. It is because the sensible heat flux (H) is known and reliable at anchor pixels (Bastiaanssen ,1998a, 2000; Waters et al., 2002). Based on equation (5), the aerodynamic resistance (r_{ah}) and the temperature difference (dT) can be calculated. In this process, the Monin Obukhov Length (L) equation (Waters et al. 2002) is used to determine the stability status of atmosphere in interactive conditions. Depending on the value of L, checking the stability of momentum and heat transport, and the friction velocity is needed. When r_{ah} and dT are stable, or the alteration is not significant, they can be accepted (Webb, 1970; Paulson, 1970; Waters et al., 2002). Because dT and T_s were assumed to be linear (equation 6), a and b can be determined on anchor pixels. Subsequently, dT can be interpolated for another pixel of the whole area in the

model based on a,b and T_s. Then, r_{ah} can be extrapolated for the entire area. Finally, the instantaneous evapotranspiration is calculated. This value is representative for ET at the times of satellite image acquisition.

To interpolate the daily actual evapotranspiration, the evaporative fraction Λ was used (Bastiaanssen 2000). Several authors also use that factor (Santos, C. A. C. et al., 2010; Sun et al., 2011; Mcebisi Mkhwanazi, 2014; Jassas et al., 2015) to estimate AE for their regions, and AE values were acceptable.

$$\Lambda = \frac{\lambda E}{(R_n - G)} \quad (7)$$

To extrapolate evapotranspiration to more extended time periods, such as one day or longer, Bastiaanssen et al., (2005) omitted G. It is because G is normal much lower than R_n. Thus, (R_n – G) was reduced to R_n; then AE is calculated as

$$AE = \frac{\Lambda R_{n24}}{\lambda \rho_w} 86400.10^3 \quad (8)$$

where AE (mm/d) is the daily actual evapotranspiration, R_{n24} (W/m^2) is the daily average net radiation, ρw is the water's density (kg/m^3), and λ is the latent heat of vaporization (J/kg).

4. RESULTS AND DISCUSSIONS

With four images free of cloud cover the results of the SEBAL model are four daily AE maps for the acquisition dates of October 28, 2006; February 1, 2007; May 8, 2007, and September 29, 2007 (Figure 3). The daily AE values vary from 0 mm/d to 6 mm/d. The maximum mean value is in May, and the minimum is in February, with 2.3 mm/d and 1.7 mm/d, respectively (Table. 1).

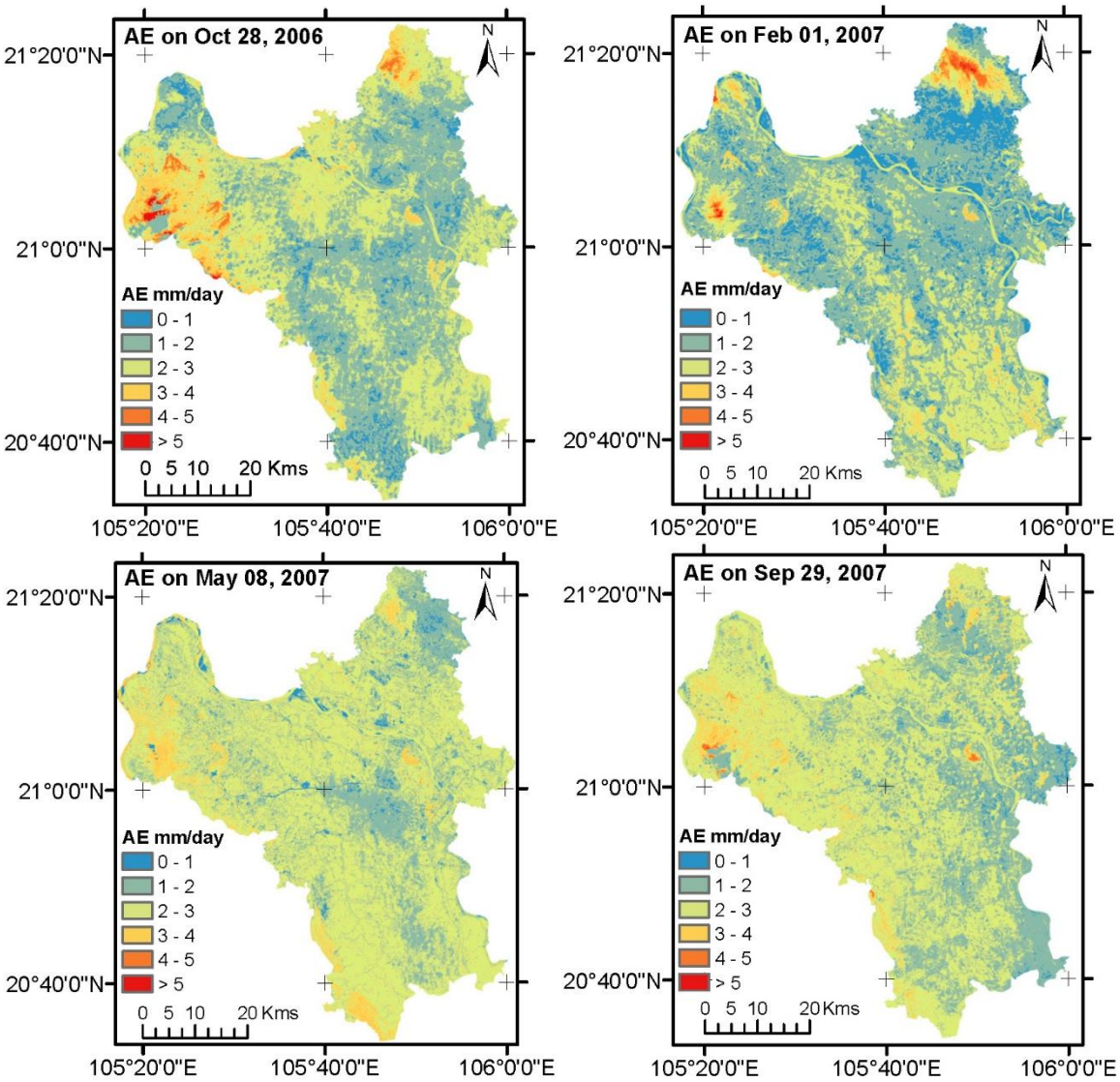

Figure. 3. Spatial and temporal distribution of AE in Hanoi calculated by means of the SEBAL model during the acquisition dates listed above each image.

This is because the temperature is high during the summer period (including May) and the number of sunshine hours is also higher than during other seasons. In the winter season (including February), the temperature is low, and humidity is highest while there is less sunshine than in other seasons. Subsequently, the mean AE will be lower during winter. In each image, the higher AE values appear above rivers, lakes and free water surfaces. This is visible in the image from February 1, 2007. Most of the agricultural land is covered by water during the period in which the new paddy rice harvest is growing. AE in February shows the lowest values despite vast free water bodies. The lowest values of AE in each image are in the congested areas, and bare soil zones where PE is high but the water quantity available for evaporation is low.

Table. 1. Statistical evaluation of the AE maps

Statistical parameters	Oct 28, 2006	Feb 01, 2007	May 08, 2007	Sep 29, 2007
Maximum (mm/d)	5.3	5.1	5.8	5.2
Arithmetic mean (mm/d)	2.1	1.7	2.3	2.2
Standard deviation	0.72	0.74	0.54	0.54
Sum (mm/d)	7,519,800	6,401,500	8,360,300	8,064,400

Figure 4, and Table 2 show the comparison of AE estimated by SEBAL and PE calculated by Penmann – Monteith equation using the meteorological data and Ep measured in four weather stations. All AE values estimated by SEBAL are lower than the corresponding PE and Ep values, which is plausible. AE accounts for 80 % to 90 % of PE and 70% to 79% of Ep. In seasonal scale, the difference of AE, PE, and Ep is not much.

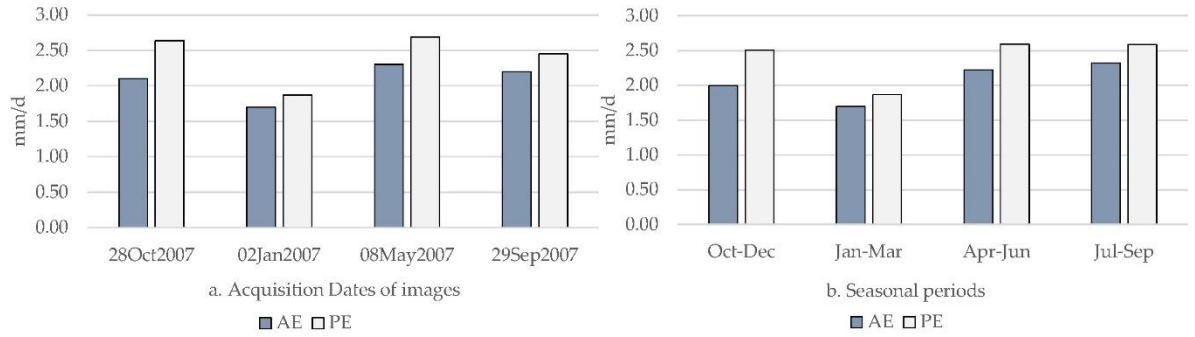

Figure. 4. Comparison of AE estimated by SEBAL and PE calculated by Penmann – Monteith equation on (a) daily and (b) seasonal scale.

The distribution of AE calculation is shown in Table. 3. AE values of 2 to 3 mm/d in three out of four images account for around 60 % of the area, while the majority AE (nearly 52 %) in the February 2007 image shows the range between 1 and 2 mm/d. Values of over 5 mm/d

Table. 2. Daily actual evapotranspiration and seasonal actual evapotranspiration

Evaporation	Daily				Seasonal			
(mm/d)	Oct 2006	Jan 2007	May 2007	Sep 2007	Oct-Dec	Jan-Mar	Apr-Jun	Jul-Sep
AE	2.1	1.7	2.3	2.2	2.0	1.7	2.2	2.3
PE	2.6	1.9	2.7	2.5	2.5	1.9	2.6	2.6
Ep	2.74	2.25	3.12	2.78	2.63	1.89	2.93	2.62

occur only in small areas making up less than 1 % of the area of interest. The mean of AE in the images on October 2006, and February 2007 (with 2.1 and 1.7 mm/d, respectively) are lower than the mean of AE on May and September 2007 (with 2.2 and 2.3 mm/d, respectively) (Table. 1). However, the areas with AE values > 5 mm/d in these images (October 2006 and February 2007) are larger (with 0.55% and 0.13%, respectively) than May and September 2007 (with 0.07 and 0.02, respectively) (Table 3). This is because there are small mountainous areas in these images (explained below).

Table. 3. Distribution of daily actual evapotranspiration in the area of interest (%).

Range of AE (mm/d)	**Oct 28, 2006**	**Feb 1, 2007**	**May 8, 2007**	**Sep 29, 2007**
0-1	1.4	14	2.4	2.4
1-2	18	52	24	33
2-3	58	30	67	59
3-4	19	3.6	6.0	5.5
4-5	3.2	0.79	0.57	0.23
> 5	0.55	0.13	0.07	0.02
Total	100	100	100	100

Although there are only four images without cloud cover available in the study area, it is assumed that they sufficiently represent the four seasonal periods in this area and that the mean seasonal values can be interpolated from these values. The mean seasonal AE values are lowest from January to March while the highest values are from April to June with 156 mm and 212 mm, respectively (Table. 4). The annual AE calculated with the SEBAL model is 751 mm (Table. 4) compared with 873 mm of PE, and 920 mm of Ep (NCHMF 1961 – 2010). AE accounts for 86 % and 82% of PE and Ep respectively.

Table. 4. The actual evapotranspiration extrapolated for one year from November 2006 to October 2007.

Statistical parameters	**October - December**	**January - March**	**April - June**	**July – September**
Minimum (mm)	0	0	0	0
Maximum (mm)	489	471	545	470
Mean (mm)	189	156	212	195

Small mountainous areas in the west and northeast of Hanoi cause a minor overestimation of AE in the three images from October 28, February 1, and September 29. This overestimation is a result of the effect of the higher altitude and its related lower temperature. The temperature difference (dT) is not equal at low and high altitude, and the aerodynamic resistance (r_{ah}) is only obtained from the wind speed at 200 meters above the surface. Wind speed at 200 meters was calculated from the wind speed at the weather station, which is not representative for the entire area including the plain and mountainous areas. That causes an error in the mountainous areas. However, this error is not a big problem, because the high values (higher than 5 mm/d) account for less than 1 % of the area. The best way to improve the AE maps is to omit the mountainous areas in the calculation or to interpolate between surrounding values. Using the first option, the error appeared with dT estimation can be minimized.

5. CONCLUSION

SEBAL was applied to estimate the AE in Hanoi for a single year. The predicted AE was compared with the PE calculated using the Penmann – Monteith equation. It is probably the first estimation of AE in the area of interest. The results seem to be plausible and consistent with the ET theory. Low values are found above the bare soil and urban areas, whereas high values appear above surface water bodies.

This study also indicates that SEBAL can be applied in humid areas and it can help to calculate the groundwater recharge for the Red River delta of Hanoi.

If AE measured in the field at certain spots is available, the estimated AE would be more accurate because then the model could be improved and calibrated with this data.

6. ACKNOWLEDGMENTS

The authors thank Ngoc C. Le, Iwona Woloszyn, Mandy Hoyer, and Daniel Suman for reviewing the manuscript and English proofreading. Authors thank the anonymous reviewers for their valuable critical comments.

7. REFERENCES

Allen, R. G., 1998, Crop evapotranspiration. Guidelines for computing crop water requirements. Rome: Food and Agriculture Organization of the United Nations (FAO irrigation and drainage paper, 56).

Allen, Richard G., Tasumi, Masahiro, Morse, Anthony, Trezza, Ricardo, Wright, James L., Bastiaanssen, Wim., 2007a, Satellite-Based Energy Balance for Mapping Evapotranspiration with Internalized Calibration (METRIC)–Applications. In *J. Irrig. Drain Eng.* 133 (4), p. 395–406. DOI: 10.1061/(ASCE)0733-9437(2007)133:4(395).

Allen, Richard G., Tasumi, Masahiro, Trezza, Ricardo, 2007b, Satellite-Based Energy Balance for Mapping Evapotranspiration with Internalized Calibration (METRIC)—Model. In *J. Irrig. Drain Eng.* 133 (4), p. 380–394. DOI: 10.1061/(ASCE)0733-9437(2007)133:4(380).

Ayman A Suleiman, Khaled M Bali, Jan Kleissl, 2009, Comparison of ALARM and SEBAL Evapotranspiration of Irrigated Alfalfa. DOI: 10.13031/2013.27033.

Bastiaanssen, W. G. M., Noordman, E. J. M., Pelgrum, H., Davids, G., Thoreson, B. P., Allen, R. G., 2005, SEBAL Model with Remotely Sensed Data to Improve Water-Resources Management under Actual Field Conditions. In *J. Irrig. Drain Eng.* 131 (1), p. 85–93. DOI: 10.1061/(ASCE)0733-9437(2005)131:1(85).

Bastiaanssen, W.G.M, 1998a, A remote sensing surface energy balance algorithm for land (SEBAL). 1. Formulation.

Bastiaanssen, W.G.M, 1998b, A remote sensing surface energy balance algorithm for land (SEBAL). 2. Validation.

Bastiaanssen, W.G.M, 2000, SEBAL-based sensible and latent heat fluxes in the irrigated Gediz Basin, Turkey. In *Journal of Hydrology* 229 (1-2), p. 87–100. DOI: 10.1016/S0022-1694(99)00202-4.

Bhaskar R. Nikam, 2014, Comparative evaluation of diffirent potential evapotranspiration estimation approaches. In *IJRET* 03 (06), p. 544–552. DOI: 10.15623/ijret.2014.0306102.

Cuxart, J., Conangla, L., Jiménez, M. A., 2015, Evaluation of the surface energy budget equation with experimental data and the ECMWF model in the Ebro Valley. In *J. Geophys. Res. Atmos.* 120 (3), p. 1008–1022. DOI: 10.1002/2014JD022296.

Di Long, Singh, Vijay P., Li, Zhao-Liang, 2011, How sensitive is SEBAL to changes in input variables, domain size, and satellite sensor? In *J. Geophys. Res.* 116 (D21). DOI: 10.1029/2011JD016542.

Djaman, Koffi, Balde, Alpha B., Sow, Abdoulaye, Muller, Bertrand, Irmak, Suat, N'Diaye, Mamadou K. (2015, Evaluation of sixteen reference evapotranspiration methods under sahelian conditions in the Senegal River Valley. In *Journal of Hydrology: Regional Studies* 3, p. 139–159. DOI: 10.1016/j.ejrh.2015.02.002.

Elhaddad, Ayman, Garcia, Luis A., 2008, Surface Energy Balance-Based Model for Estimating Evapotranspiration Taking into Account Spatial Variability in Weather. In *J. Irrig. Drain Eng.* 134 (6), p. 681–689. DOI: 10.1061/(ASCE)0733-9437(2008)134:6(681).

Elizabeth A. H. and Robert E. C., 2013, Water Balance Estimates of Evapotranspiration Rates in Areas with Varying Land Use: InTech.

Farah, Hussein O., Bastiaanssen, Wim G. M., 2001, Impact of spatial variations of land surface parameters on regional evaporation. A case study with remote sensing data. In *Hydrol. Process.* 15 (9), p. 1585–1607. DOI: 10.1002/hyp.159.

Hargreaves, G.H., and Samani, Z.A, 1985, Reference crop evapotranspiration from temperature (Appl. Eng. Agric. 1 (2), 96–99).

Hoekstra, T. W., Shachak, M., 1999, Arid Lands Management: Toward Ecological Sustainability: University of Illinois Press. Available online at https://books.google.de/books?id=yWgQv1NhdZkC.

Jacobs, Jennifer M., Satti, Sudheer Reddy, 2001, Evaluation of reference evapotranspiration methodologies and AFSIRS crop water use simulation model. Final report. [Palatka, Fla.]: [St. Johns River Water Management District] (Special publication, SJ2001-SP8).

Jassas, Hussein, Kanoua, Wael, Merkel, Broder, 2015, Actual Evapotranspiration in the Al-Khazir Gomal Basin (Northern Iraq) Using the Surface Energy Balance Algorithm for Land

(SEBAL) and Water Balance. In *Geosciences* 5 (2), p. 141–159. DOI: 10.3390/geosciences5020141.

Martin Jung, 2010, Recent decline in the global land evapotranspiration trend due to limited moisture supply. *Nature 467, 951–954* (21 October 2010). DOI: 10.1038/nature09396.

Khalili, N., Russell, A., Khoshghalb, A., 2014, Unsaturated Soils: Research & Applications: Taylor & Francis. Available online at https://books.google.de/books?id=_O3MAwAAQBAJ.

Kustas, William P., Norman, John M., 2000, A Two-Source Energy Balance Approach Using Directional Radiometric Temperature Observations for Sparse Canopy Covered Surfaces. In *Agronomy Journal* 92 (5), p. 847. DOI: 10.2134/agronj2000.925847x.

Le, Thi Phuong Quynh, Seidler, Christina, Kändler, Matthias, Tran, Thi Bich Nga, 2012, Proposed methods for potential evapotranspiration calculation of the Red River basin (North Vietnam). In *Hydrol. Process.* 26 (18), p. 2782–2790. DOI: 10.1002/hyp.8315.

Liou, Yuei-An, and Kar, Sanjib, 2014, Evapotranspiration Estimation with Remote Sensing and Various Surface Energy Balance Algorithms—A Review. In *Energies* 7 (5), p. 2821–2849. DOI: 10.3390/en7052821.

Mcebisi Mkhwanazi, 2014, Developing a modified SEBAL algorithm that is responsive to advection by using limited weather data. Colorado State University, Fort Collins, Colorado.

Monteith, John Lennox, Unsworth, M. H., 1990, Principles of environmental physics. 2nd ed. London, New York, New York: E. Arnold, Distributed in the USA by Routledge Chapman and Hall.

NCHMF, 1961-2010, National Centre for Hydro-Meteorological Forecasting of Viet Nam. Annual reports on Hydro-meteorology of Viet Nam.

Nguyen V. Lam, Nguyen K. Ngoc, Nguyen T. Tien, Pham H. Anh, Vu V. Hung., 2012, Investigating, evaluating and determining the prohibited, limited or allowed exploitation areas for Hanoi capital. Hanoi Environment and Natural Resources Department.

Oki, Taikan, Kanae, Shinjiro, 2006, Global hydrological cycles and world water resources. In *Science (New York, N.Y.)* 313 (5790), p. 1068–1072. DOI: 10.1126/science.1128845.

Paron, P., Di Baldassarre, G., Shroder, J. F., 2014, Hydro-Meteorological Hazards, Risks, and Disasters: Elsevier Science. Available online at https://books.google.de/books?id=0FtzAwAAQBAJ.

Paulson, C.A, 1970, The Mathematical Representation of Wind Speed and Temperature Profiles in the Unstable Atmospheric Surface Layer.

Roerink, G.J, Su, Z., Menenti, M., 2000, S-SEBI. A simple remote sensing algorithm to estimate the surface energy balance. In *Physics and Chemistry of the Earth, Part B: Hydrology, Oceans and Atmosphere* 25 (2), p. 147–157. DOI: 10.1016/S1464-1909(99)00128-8.

Santos, C. A. C., Bezerra, Bergson Guedes, Silva, Bernardo Barbosa da, Rao, Tantravahi Venkata Ramana, 2010, Assessment of daily actual evapotranspiration with SEBAL and S-SEBI algorithms in cotton crop. In *Rev. bras. meteorol.* 25 (3), p. 383–392. DOI: 10.1590/S0102-77862010000300010.

Senay, G. B., Leake, S., Nagler, P. L., Artan, G., Dickinson, J., Cordova, J. T., Glenn, E. P., 2011, Estimating basin scale evapotranspiration (ET) by water balance and remote sensing methods. In *Hydrol. Process.* 25 (26), p. 4037–4049. DOI: 10.1002/hyp.8379.

Senay, G. B., Verdin, J. P., Lietzow, R., Melesse, A. M., 2008, Global Daily Reference Evapotranspiration Modeling and Evaluation 1. In *JAWRA Journal of the American Water Resources Association* 44 (4), p. 969–979. DOI: 10.1111/j.1752-1688.2008.00195.x.

Sobrino, J. A., 2002, Recent Advances in Quantitative Remote Sensing: Publicacions de la Universitat de València. Available online at https://books.google.de/books?id=aTiFwbmraYoC.

Su, Z., 2002, The Surface Energy Balance System (SEBS) for estimation of turbulent heat fluxes. In *Hydrol. Earth Syst. Sci.* 6 (1), p. 85–100. DOI: 10.5194/hess-6-85-2002.

Sun, Zhongping, Wei, Bin, Su, Wei, Shen, Wenming, Wang, Changzuo, You, Daian, Liu, Zheng, 2011, Evapotranspiration estimation based on the SEBAL model in the Nansi Lake Wetland of China. In *Mathematical and Computer Modelling* 54 (3-4), p. 1086–1092. DOI: 10.1016/j.mcm.2010.11.039.

Turc, L., 1961, Water requirements assessment of irrigation, potential evapotranspiration: Simplified and updated climatic formula Annales Agronomiques, p. 12, 13-49.

VUSTA, Ed., 2012, Workshop: Groundwater exploitation reserves in Hanoi area and Solutions for water supply. Vietnam Union of Science and Technology Associations (VUSTA).

Waters, R., Allen R, Bastiaanssen W, 2002, SEBAL. Surface Energy Balance Algorithms for Land. Idaho Implementation. Advanced Training and Users Manual, Idaho, USA.

Webb, E. K., 1970, Profile relationships. The log-linear range, and extension to strong stability. In *Q.J Royal Met. Soc.* 96 (407), p. 67–90. DOI: 10.1002/qj.49709640708.

Wilm, H. G., Thornthwaite, C. W., Colman, E. A., Cummings, N. W., Croft, A. R.; Gisborne, H. T. (1944, Report of the Committee on Transpiration and Evaporation, 1943–44. In *Trans. AGU* 25 (5), p. 683. DOI: 10.1029/TR025i005p00683.

Integrated approach to forecast future suspended sediment load by means of SWAT and artificial intelligence models, a case study

Mustafa Al-Mukhtar Building and Construction Engineering Department, University of Technology. Baghdad, Iraq. mmalmukhtar@gmail.com

Abstract

Estimation and projection of Suspended Sediment Load (SSL) is critically important in a successful application of water resources management. This study introduces a novel method applied on a case study (upper reach of the Spree River in Germany) to project future SSL by integrating Artificial Intelligence (AI) with the Soil and Water Assessment Tool (SWAT) model. The AI methods encompass Adaptive Neuro Fuzzy Inference System (ANFIS), feedforward, cascade feedforward, pattern recognition, radial basis, generalized regression and layer recurrent neural networks. They were evaluated to model SSL using streamflow discharges as inputs. Subsequently, the optimal structure from the above methods was used to estimate the amounts of seasonal and yearly SSL transported by the river during the period 1997-2006. The future climate change data obtained from regional climate change model (CLM-A1B) was used as inputs to the calibrated SWAT model to project the near future discharges through two periods (2021-2030 and 2041-2050). Lastly, the impact of climate changes on SSL was assessed by employing future discharges to the best evaluated method. Results revealed that the ANFIS model outperformed all the other methods. R^2 and RMSE of ANFIS during the validation period were equal to 0.60 and 87.41 mg/l, respectively. The SSL was projected to decrease by almost 76% and 57% during 2021-2030 and 2041-2050, respectively with respect to the period 1997-2006.

Keywords: modelling; suspended sediment; artificial intelligence; prediction; risk analysis

1 Introduction

Estimating and predicting suspended sediment load (SSL) in rivers is of particular interest in management of water resources, as the estimated load is commonly needed in wide spectrum fields of water resources engineering such as planning of reservoirs, watershed management, and ecological assessment etc. The traditional calculation of sediment yield is by relating sediment concentration to river flow values through a nonlinear relationship. Hence, a few sediment data could be extrapolated up to the length of the discharge records (Cigizoglu and Kisi 2006). Given the high intricacy, dynamism, and non-stationarity of

suspended sediment loads; the artificial intelligence (AI) methods have demonstrated the ability to overcome these inherent dilemmas (Afan et al. 2016).

Adaptive Neuro Fuzzy Inference System (ANFIS) has been one of the superior techniques used in water resources field (Rajaee et al. 2009; Maiti and Tiwari 2014; Kisi and Zounemat-Kermani 2016; and may others). ANFIS, which is a fuzzy inference system implemented in the frame of adaptive networks using a hybrid learning procedure, can be constructed to mapping input-output relationship based on both human knowledge and stipulated input-output data pairs (Jang 1993). ANFIS has been used in many environmental and hydrological related problems (El-Shafie et al. 2007; Afan et al. 2016). However, few studies used ANFIS to model the suspended load- river discharge nonlinear- relationship. This relationship is of great importance to be addressed, because mostly the suspended loads are measured instantaneously along with discharges. Besides that, developing a predictive model of sediment transport based on minimal input is essential and necessary.

The artificial neural network (ANN) approach as a non-linear black box model would seem typically a useful technique for modelling a complex relation between dependent and independent variables. Many successful applications of the ANNs in the field of water resources have been reported in the literature such as the rainfall runoff relationship (Mason et al. 1996; Minns and Hall 1996; Fernando and Jayawardena 1998), river flow prediction (Tokar and Johnson 1999; Cigizoglu 2005; Kisi and Cigizoglu 2007; Chen et al. 2015), rainfall estimation (Luk et al. 2000; Luk et al. 2001; Ramírez et al. 2005), groundwater (Daliakopoulos et al. 2005; Lallahem et al. 2005), and water quality (Wen and Lee 1998; Palani et al. 2008; Rai and Mathur 2008; Singh et al. 2009). The application of ANNs to SSL data has been recently increased (Jain 2001; Nagy et al. 2002; Tayfur 2002) and many others. For example, Alp and Cigizoglu (2007) used the feed-forward back-propagation (FFBP) method and the radial basis functions (RB) to estimate the daily total SSL. They trained neural networks using different hydro meteorological data from the Juniata Catchment, USA. They concluded that the ANNs provided satisfactory simulations in terms of the selected performance criteria and comparable to the conventional multi-linear regression against the observed data. Rajaee et al. (2009) evalauted feedforward, neuro-fuzzy (NF), multi linear regression (MLR) and conventional sediment rating curve (SRC) models. They demonstrated that ANN could improve the accuracy of modelled suspended sediment over the MLR and SRC. However, Most of the previous studies of the ANNs focused on using feedforward or radial basis neural networks to model suspended sediment. As a result, this study investigates a wider spectrum of the available ANNs methods. Moreover, none of the aforementioned methods has attained universal

acceptance for SSL prediction. Therefore, an accurate modelling of the river SSL, based on local data, is essential to improve the prediction of suspended sediment. Consequently, this prediction could serve as a tool for better water management in terms of risk analysis. The ultimate objective of this study is to approximate future SSL in the upper reach of the Spree River in Germany using a novel method. To achieve that, in the first part, the aim was to investigate the capability and accuracy of AI methods to model SSL in the study area using the streamflow discharge as input. To this end, results from ANFIS, ANNs (including feedforward, cascade feedforward, pattern recognition, radial basis, generalized regression and layer recurrent) and sediment-rating curve were compared. The evaluated methods were selected to insure involving the various types of ANNs i.e. static, statistical, and dynamical networks. Thereafter, the best structure of AI was used to estimate the seasonal and yearly amounts of SSL over the period 1994-2010. In the second part, the Soil and Water Assessment Tool (SWAT) and the best-evaluated method from the AI models were integrated to model the impacts of climate changes on suspended load in the study area. To this end, the SWAT model was calibrated and validated against daily streamflow for a rather long term period (1997-2010). Consequently, future streamflow were projected through re-running the calibrated SWAT model with the future climate data from the regional climate change model (CLM) under SRES-A1B scenario. Finally, the future discharges were fed as inputs to the best-evaluated method of the AI models to estimate the suspended sediment concentration during two near future periods (2021-2030 and 2041-2050).

2 Study area and data

The upper reach of the Spree River is a 310-km^2 catchment located at the eastern part of Germany between 14° 36′ 32″ and 14° 26′ 24″ longitude and 51° 14′ 3″ and 50° 58′ 9″ latitude. The catchment stretches from the Czech Republic border in the south to the Bautzen reservoir in the North West. The range of the watershed topography is from 154 to 563 m above mean sea level and slopes from 0% to 30.2%. The average annual precipitation is about 730 mm, mainly falls in the form of rainstorms from May to September (maximum in July and August) (Al-Mukhtar 2016). The collected data in this study were streamflow (m^3/sec) with its corresponding SSL (mg/l) measured instantaneously on discrete intervals (with at best one measurement per month) for the Spree River at the Bautzen gauge for the period 1993-2011. In total 270 values of both discharge and suspended sediment were available. These values were obtained from the water quality management of national reservoir management of Saxony.

3 Methods for modelling suspended sediment concentration

Because the streamflow and suspended sediment concentrations are not typically measured simultaneously and continuously, it is of great importance in water management to find a reliable estimator of SSL. Using the raw data (streamflow and suspended sediment concentration, (SSC)), two data sets were derived: one for model training and the other for model validation. 75% of the data employed for model training and the remainder 25% for the model validation. Table 1 shows the descriptive statistics of suspended sediment concentration during both training and validation periods. The sediment series has a quite high variability (STD=113.74), positive skew (Csx=7.51), and mean value of 36.0 mg/l. For the entire period, the first quartile of suspended sediment was equal to 7 mg/l, the third quartile was 19 mg/l, and the median was 10 mg/l. Given that the mean for the entire period is 36.0 mg/l, the highest flow of 1300 mg/l is more deviant from the mean than the lowest flow of 1 mg/l. Therefore, it was considered as an outlier and eliminated (McCuen 2002). Once the training process was completed, the performance of the trained network was validated subsequently against known independent values to assess the generalization ability using the chosen criteria (Dawson and Wilby 2001). The performance of the methods is satisfactorily accepted when they reveal satisfactory results of the assessment criteria during both the training and validation. All the computations were done with the use of MATLAB software (R2008a), ANFIS, artificial neural network modelling, and the regression analysis. The following section describes the methods of suspended sediment modelling used in this study.

Table 1 Descriptive statistics of suspended sediment concentration mg/l

	Min	Max	Mean	Median	STD	Csx
Calibration	1	1300	30.8	10	110.50	8.77
Validation	1	860	50.91	16	122.12	4.87

3.1 Adaptive neuro fuzzy inference system (ANFIS)

ANFIS is a special type of ANNs that integrates both neural networks and fuzzy logic principles (Jang 1993). It is considered an universal approximation system because it has the capability of approximating any real continuous function on a compact set of data to any degree of accuracy using mostly either Takagi–Sugeno or Mamdani fuzzy inference system (if-then rule) (Jang et al. 1997). Takagi and Sugeno's fuzzy if-then rules are characterized as the output of each rule is a linear combination of the input

variables plus a constant term, and the final output is the weighted average of each rule's output (Jang 1993). A hybrid-learning rule, which is a combination of the gradient method and the least squares estimate, which is employed to identify parameters pertaining membership function (MF), was adopted to be used in ANFIS because it is faster and not trapped by local minima as in the basic rule. As a typical example, it is assumed a fuzzy inference system with two input variables (x and y) and one output f. The first-order Sugeno's fuzzy model, a typical rule set with two fuzzy If-Then rules can be written as:

Rule 1: If x is A_1 and y is B_1; then $f_1 = p_1x + q_1y + r_1$ **1**

Rule 2: If x is A_2 and y is B_2; then $f_2 = p_2x + q_2y + r_2$ **2**

p_1, q_1, r_1 and p_2, q_2, r_2 are the parameters in the then-part (consequent part) of the first-order Sugeno fuzzy model. The general structure of ANFIS is shown in Figure 1. A comprehensive details about ANFIS functioning can be found in Jang (1993). In this study, each run with different numbers of member functions (MF) was tried and the one that gave the minimum squared error was selected. Triangular-shaped built-in MFs for the ANFIS models were found to be efficient for modelling SSL in the upper reach of the Spree River.

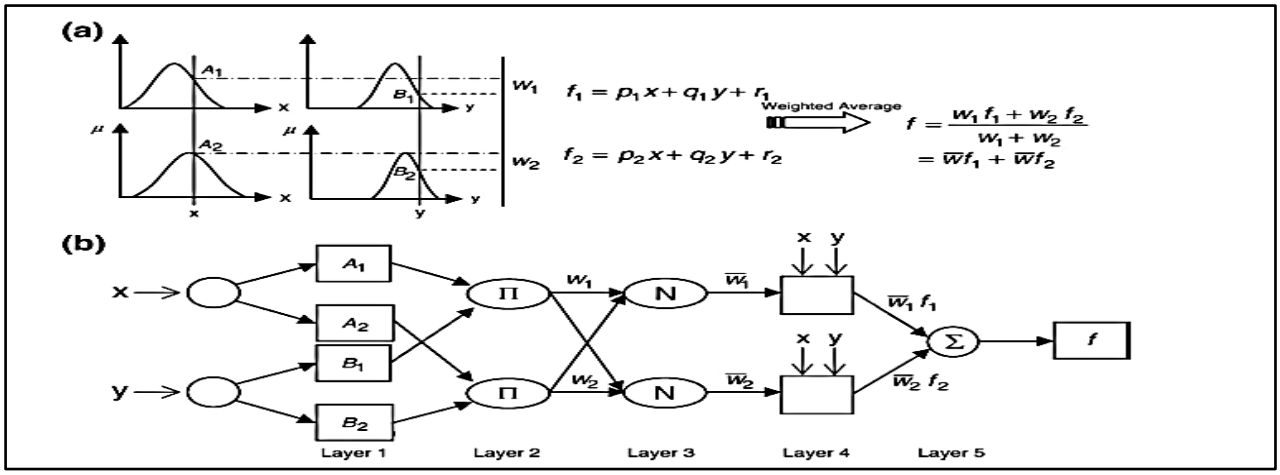

Figure 1 (a) Sugeno's fuzzy reasoning mechanism (b) equivalent ANFIS structure (adopted from Jang 1993)

3.2 Artificial neural network models

Artificial neural network is one of the most robust tools used in modelling the nonlinear relationships between inputs and targets. Researches on the brain and nervous systems in living organisms were behind the inspiration of its computational approach (Luk et al. 2001). The robust functionality of a biological neural system is due to the parallel-distributed processing nature of a network of cells (neurons). Hence, an ANN mimics this structure by distributing the computation to processing units, called artificial neurons, or nodes. Through the interaction of these neurons, the ANN can be used to complete information processing of the network (Feng and Lu 2010). Therefore, an ANN has proven to be a powerful mathematical model, that have the advantages of self-learning, self-organizing, and self-adapting (Feng and Hong 2008; ASCE Task Committee on Application of Artificial Neural Networks 2000b). The individual ANNs used in the modelling of suspended sediment concentration are described briefly in the following sections, more detailed can be found in Beale et al. (2012).

3.2.1 Feedforward neural network

Feedforward neural network *(FF)* is a multi-layer perceptron type where nodes in one layer are only connected to nodes in the next layer, it has been used for prediction and forecasting applications (Maier and Dandy 2000). Typically, feedforward networks have one or more hidden layers of sigmoid transfer function followed by an output layer of linear transfer function. Nonlinear transfer functions in multiple layers of neurons allow the network to learn nonlinear and linear relationships between input and output vectors. The linear output layer makes the network to produce values outside the range -1 to +1 (Beale et al. 2012). A supervised learning technique called backpropagation is used to train the network. The backpropagation computation is derived using the chain rule of calculus (Hagan et al. 1996). The default algorithm used in optimizing weights between connections is Levenberg-Marquardt backpropagation (Hagan et al. 1996).

3.2.2 Cascade feedforward neural network

Cascade feedforward neural network (CFF) has a similar configuration of feedforward, except that it includes a connection from the input and every previous layer to the following layers (Beale et al. 2012). In addition, the transfer function used in output layer is a hyperbolic tangent sigmoid transfer function instead of linear function in a feedforward network.

3.2.3 Pattern recognition neural network

The pattern recognition neural network (PR) is also derived from the feedforward network, but it is trained to classify inputs according to target classes (Beale et al. 2012; Dumedah et al. 2014). Moreover, a hyperbolic tangent sigmoid transfer function is used in both hidden and output layers. Thus, the classification output will range between -1 and 1, giving wider categories of outputs.

3.2.4 Radial basis neural network

Radial basis networks (RB) typically have three layers: an input layer, hidden layer with non-linear radial basis function (RBF), and linear output layer. The RBF estimates the output by using the standard Euclidean distance between the inputs and its corresponding weight (ASCE Task Committee on Application of Artificial Neural Networks, 2000a; Beale et al. 2012). In other words, for each node the Euclidean distance between the centre and the input vector is estimated, and then transformed by a non-linear function (Exponential) that determines the output from the hidden layers. The radial basis function has a maximum of 1 when its input is 0. When the distance between the weight (**w)** and input (**p)** decreases, the output increases. Thus, a radial basis neuron acts as a detector that produces 1 whenever the input **p** is identical to its weight vector **w**.

3.2.5 Layer recurrent neural network

The layer recurrent (LR) (also known as Elman neural network) is a dynamic type of neural networks (Elman 1990). Although it has three-layers as in feedforward type, this type is characterized by feedback loop having a single delay in every layer except the output layer. In other words, input neurons are linked to a hidden neuron, where each hidden neuron has its corresponding time-delay unit. Its output depends on the current input information and on the previous states of the network. The same algorithm of FF (i.e. Levenberg–Marquardt back propagation) is used to train the Elman neural network. The sigmoid and linear transfer functions are used in hidden and output layers, respectively.

3.2.6 Generalized regression neural network

The generalized regression network (GR) has a similar configuration as the radial basis network: it sets the radial basis function in the first layer, but with slightly different second layer (Beale et al. 2012). The GR neural network consists of four layers: input layer, pattern layer, summation layer and output layer. It uses net input functions in the second layer that calculates a layer's net input by combining its weighted inputs

and biases. Moreover, the number of nodes can be as many neurons as the inputs. The GR network is used for estimation of continuous variables, as in standard regression techniques. It is related to the radial basis function network and is based on a standard statistical technique called kernel regression.

The optimal number of neurons in the hidden layer of feedforward type network was determined using trial and error procedure. The range of tested neurons number was in the range 5 to 20. Subsequently, the optimal number of neurons and its trained network were used to model the suspended sediment concentrations for validation period with their known values. To ensure that all inputs and targets of the neural networks are on the same scale and thus accelerate convergence, a standardization (Equation 3) was performed on the assumption that the data always fall within a specified range (i.e., in the interval [-1, 1]).

$$\mathbf{y} = (\mathbf{y}_{max} - \mathbf{y}_{min}) \times \frac{\mathbf{x} - x_{min}}{x_{max} - x_{min}} + \mathbf{y}_{min} \quad 3$$

Where: y is the target and x is the input. max and min are maximum and minimum values, respectively.

3.2.7 Conventional regression

Conventional regression methods are fitted to data either by linear or non-linear least square regression. One of the most commonly used method in estimating suspended sediment concentration is the sediment-rating curve (SRC). The resulting rating curve is defined as an empirical relationship between streamflow and concentration. The most common regression equation is the log-log linear rating curve (Quilbé et al. 2006):

$$\log_{10} S = a + b \log_{10} Q \quad 4$$

S is the suspended sediment concentration in mg/l or ppm; Q is the river flow m^3/s, a and b are constants.

4 Methodology for predicting future streamflow

In order to predict the impact of climate changes on SSL in the study area, it is essentially to obtain the projected future streamflow during the two evaluated periods (2021-2030 and 2041-2050). To this end, the period 1997-2006 was employed to calibrate the SWAT model and the period 2007-2010 for validation using daily stream flow at the watershed outlet. Sequential uncertainty fitting (SUFI-2) (Abbaspour et al. 2004, 2007) was used for calibration, validation, uncertainty assessment in the model outputs. Then, the

calibrated model was re-run with the future climate data from the CLM model under the SRES-A1B scenario. Hence, future discharges for the two evaluated periods (2021-2030 and 2041-2050) were obtained. These discharges were used further as inputs to the best structure of the AI models to estimate the future suspended load. Daily precipitation, daily maximum and minimum temperature were used as input to SWAT from the future climate model under the SRES A1B scenario to predict the impact of future climate change on streamflow. The built-in weather generator of SWAT was applied to predict the other meteorological data. The regional climate model (CLM model) was downscaled from the global circulation model ECHAM + MPI-OM (Roeckner et al. 2003, 2006). The CLM model encompasses of two realizations: CLM-1 and CLM-2. In this study, only the CLM-1 was used to predict the impact of climate change as it show the highest values of discharges and precipitation among the others realizations (Al-Mukhtar et al. 2014). Hence, it represents the worst scenario for sediment amounts prediction. The precipitation bias in CLM climate data was corrected by calculating a multiplicative scaling of average monthly precipitation between the observations and the CLM model for the period 1991–2010. Then, this scale was applied to approximate climate data of the CLM model.

5 Soil and Water Assessment Tool (SWAT) setup

The ArcSWAT interface for SWAT 2009 (Winchell et al. 2010) was used to set up the hydrological model. To this end, a 50 m SRTM digital elevation model, soil and a land use layers from the Saxon State Office for Environment were used to build the model. The study area was then discretized into twenty-nine sub-catchments using the default threshold channel area of 6.13 km^2. Subsequently, 342 hydraulic response units (HRU's) for the entire catchment were created. The source of the meteorological data (precipitation, max. and min. temperature, relative humidity, solar radiation, and wind speed) were from the Regional Climate Information System for Saxony, Saxony-Anhalt and Thuringia website (ReKIS). The daily stream flow and suspended sediment data were obtained for the outlet catchment gauge from the Water Quality Management of National Reservoir Management database of Saxony. The calibration (1997-2006) and validation (2007-2010) periods of the SWAT model were optimized before assessing the impact of climate change on the streamflow. A spin-up period of two years (1995–1996) was used just to initiate the hydrological parameters of the watershed and was not included in the results. With respect to applying the calibration procedure, SUFI-2 was used to generate 1000 parameter combinations for each iteration from the assigned range of each parameter. Thereafter, SUFI-2 was run and the goodness of fit and uncertainty measures were calculated, and hence new parameter ranges were set. The best parameters ranges were determined at the optimal objective function after six iterations (6000 runs).

6 Evaluation criteria of AI models performance

Two most widely used criteria were applied in order to assess the goodness of fit between observed and modelled data, which are:

1. Determination coefficient (R^2): the determination coefficient (equation 5) describes the proportion of the variance in observed data explained by the model. Its values range from 0 to 1. Higher values indicate less error variance and typically values greater than 0.5 are considered acceptable (Santhi et al. 2002; Van Liew et al. 2003; Moriasi et al. 2007).

$$\mathbf{R^2} = \left[\frac{\sum_{i=1}^{n}(O_i-\bar{O})(P_i-\bar{P})}{\sqrt{\sum_{i=1}^{n}(O_i-\bar{O})^2}\sqrt{\sum_{i=1}^{n}(P_i-\bar{P})^2}}\right]^2 \qquad 5$$

Where O_i is the actual value, $\bar{O}$ is the average actual value, P_i is the predicted value, and $\bar{P}$ is the average predicted value.

2. Root mean square error (RMSE): root mean square error (equation 6) is one of the error indices commonly used in model evaluation. The closer value to zero, the better model performance.

$$\mathbf{RMSE} = \sqrt{\frac{\sum_{i=1}^{n}(O_i-P)^2}{n}} \qquad 6$$

7 Results and discussion

7.1 Evaluation of suspended sediment modelling methods

The evaluation of the AI methods was performed on two stages; calibration or training, and validation. The validation set is used to evaluate the model against independent data. The best model was determined based on its performance during both the calibration and validation stages. The scatter plots of the observed and modelled SSC with the evaluated AI methods during calibration and validation periods were depicted along with the 1:1 line in Figures 2, 4, and 5. The values of performance criteria based on R^2 and RMSE for the evaluated methods were listed in Table 2. The determination coefficient of a value > 0.5 was pointed as a satisfactory for suspended sediment modelling (Quilbé et al. 2006). According to Table 2 and based on the training data set, ANFIS configuration provided the best efficiency of modelling SSC with R^2 of 0.72 and RMSE of 33.74 mg/l. Moreover, Figure 2a shows the scatter plot between observed

and modelled suspended load from ANFIS during calibration. It can be seen from Figure 2a that the points were closely distributed along the 1:1 line except the high amounts of SSL, where they were underestimated. Figure 3a shows the observed and modelled data from ANFIS. It can be seen, that the observed peak values were consistent with those from ANFIS. The reason behind superior positive results from ANFIS might be attributed to its structure and the capability of eliminating the noisy data (Rajaee et al. 2009). On the other side, all the ANNs have an overall R^2 greater than 0.5 and RMSE less than 100 mg/l. The descending order of the ANN methods during the training was radial basis, pattern recognition, cascade feedforward, layer recurrent, feedforward, and generalized regression (Table 2). The scatter plots between the observed and modelled SSL for the FF, CFF, PR, LR, GR, and SRC were plotted as shown in Figures 4a, b, c, d, e, and f, respectively. It can be noticed from those above figures that the high amounts of SSL were consistently underestimated. This could be attributed to the complex non-linear relationship governing sediment transport process. While, for low and medium values, the scattered points are distributed uniformly around the line 45°. However, the generalized regression neural network has the worst performing among the remaining ANN methods during the training period with R^2 and RMSE equal to 0.60 and 61.11 mg/l, respectively. This could be attributed to the fact that the GRNN uses standard statistical regression that is minimizing the mean square error between the observed and modelled SSL. Using the statistical regression analysis, the sediment-rating curve or the conventional regression was able to predict only 60% from the variability in the observed data with RMSE of 40.53 mg/l. In overall, the performance of the evaluated methods during the training period show that the ANFIS and the artificial neural networks have the highest estimation accuracy and thus they can be further used to model the suspended sediment concentration using independent data set during the validation period.

During the validation procedure, the known SSC records and the modelled values from the evaluated methods were compared. The scatter plot between observed and modelled values from ANFIS during the validation is shown in Figure 2b. Besides, Figure 3b shows the observed versus modelled SSL from ANFIS. It can be seen from those figures that ANFIS was capable to nicely predict the SSC values during the validation period. R^2 and RMSE of the modelling results with ANFIS were equal to 0.60 and 87.41 mg/l, respectively. The higher performance of ANFIS could be attributed to its structure that achieved a smaller convergence error. In other words, it not only uses the advantage of the simplifying function of fuzzy reasoning, but also uses the self-learning ability of neural networks with the strong capability of eliminating noise (Rajaee et al. 2009). The remainder ANN's and the conventional regression performed poorly despite they have a value of R^2 greater than 0.50 but higher RMSE values than ANFIS

(Table 2). Figures 5a, b, c, d, e, f show the scatter plots of observed and modelled SSL from the FF, CFF, PR, LR, GR, and SRC, respectively. The performances of these methods were inconsistent due to the different algorithms used. For the feedforward methods, the descending order of performance based on RMSE is CFF, PR, and FF. These methods use the same transfer function for the hidden layer (linear) but different transfer function for the output layer. PR uses the hyperbolic tangent sigmoid as transfer function in the output layer which could be better suited for modelling SSL than the linear transfer function. The dynamic neural network type (LRNN) has rather higher estimation accuracy with R^2 and RMSE of 0.51 and 142.02, respectively. Dumedah et al. (2014) pointed out that the higher estimation accuracy of the recurrent layer network might be attributed to its evaluation of the feedback between layers through discrete time non-linear estimation.

With respect to the radial basis methods, i.e. RB and GRNN, the latter has higher estimation accuracy than RB. In overall, regression based neural network is preferred on the other networks in modelling SSL. In their study, Cigizoglu and Alp (2006) pointed out that "the GRNN performances were quite satisfactory providing close or sometimes even superior performances compared with FF in sediment estimation in terms of the selected performance criteria" and hence eliminates the negative value, which are physically unexplainable as in the FFBP applications. However, GRNN in this study was unable to capture the behaviour of suspended sediment during the validation period.

It is well known that the ANNs models are unable to extrapolate beyond the range of the data used for training (Flood and Kartam 1994; Minns and Hall 1996). Additionally, when the validation data contain values outside the range of those used for training; poor predictions can be expected. In other words, it is necessary that the training and validation sets are representative of the same population. Moreover, it is noteworthy that the ANNs are highly dependent on the amount of trained data to generate prediction. These drawbacks might represent the limitation of using ANNs in prediction procedure and could explain the unsatisfactory performance of the ANN's in this study.

On the other side, traditional SRCs performed inadequately (R^2 <0.5 and RMSE 88.50) due to the over-simplification of relating suspended sediment concentration solely to discharge. Instead, the multitude of acting processes required more flexibility to model these nonlinear relationships. In previous study, Shiau and Chen (2015) pointed out that "the sediment rating curve is insufficient to describe the inevitable scatter between sediment and discharge". However, this study shows that the ANFIS outperformed the traditional sediment-rating curve, the static, dynamic and statistical artificial neural

networks to modelling suspended sediment load. This study proved that ANFIS has the priority, in preference to the other evaluated methods, to be used as predictor of the suspended sediment concentration using the streamflow discharge as independent value.

Table 2 performance criteria of the evaluated methods

	Training		Validation	
Modelling methods	R^2	RMSE	R^2	RMSE
ANFIS	0.72	33.74	0.60	87.41
feedforward neural network	0.68	36.27	0.62	166.44
cascade forward neural network	0.71	34.09	0.51	121.31
pattern recognition neural network	0.71	33.99	0.57	132.24
radial basis neural network	0.90	33.55	0.61	4.70E+04
layer recurrent network	0.71	34.90	0.51	142.02
generalized regression neural network	0.60	61.11	0.30	118.52
conventional regression	0.60	40.53	0.48	88.50

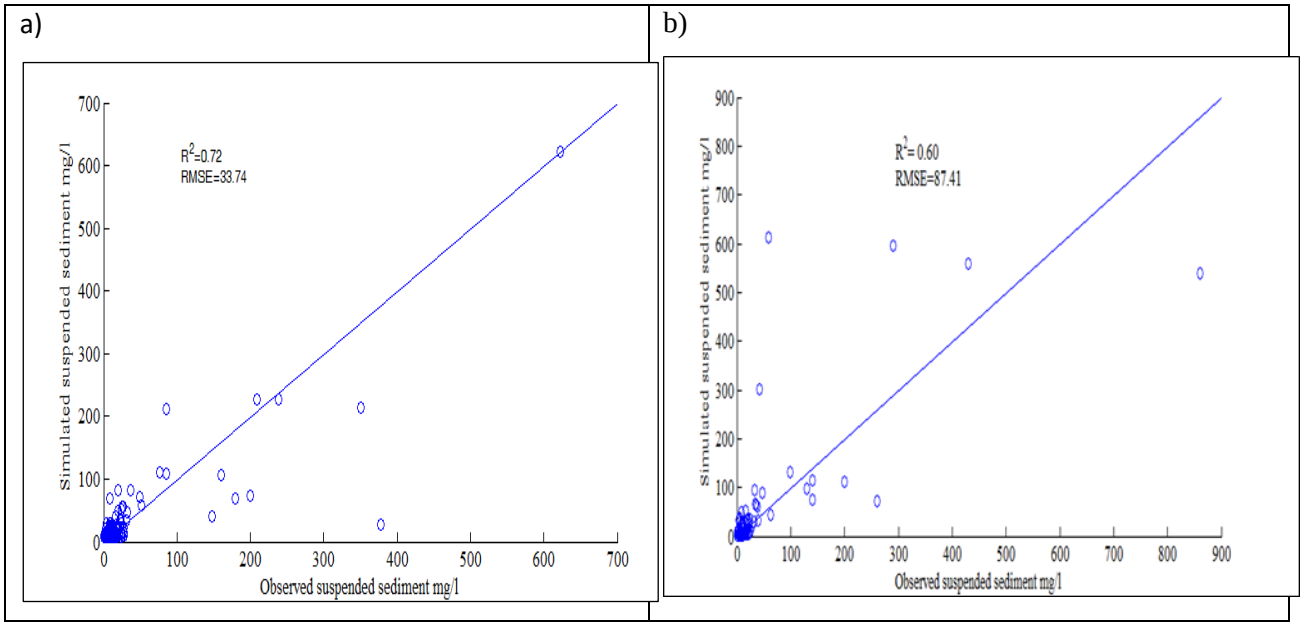

Figure 2 Comparison of observed and modelled suspended sediment from ANFIS in the **a)** training period **b)** validation period

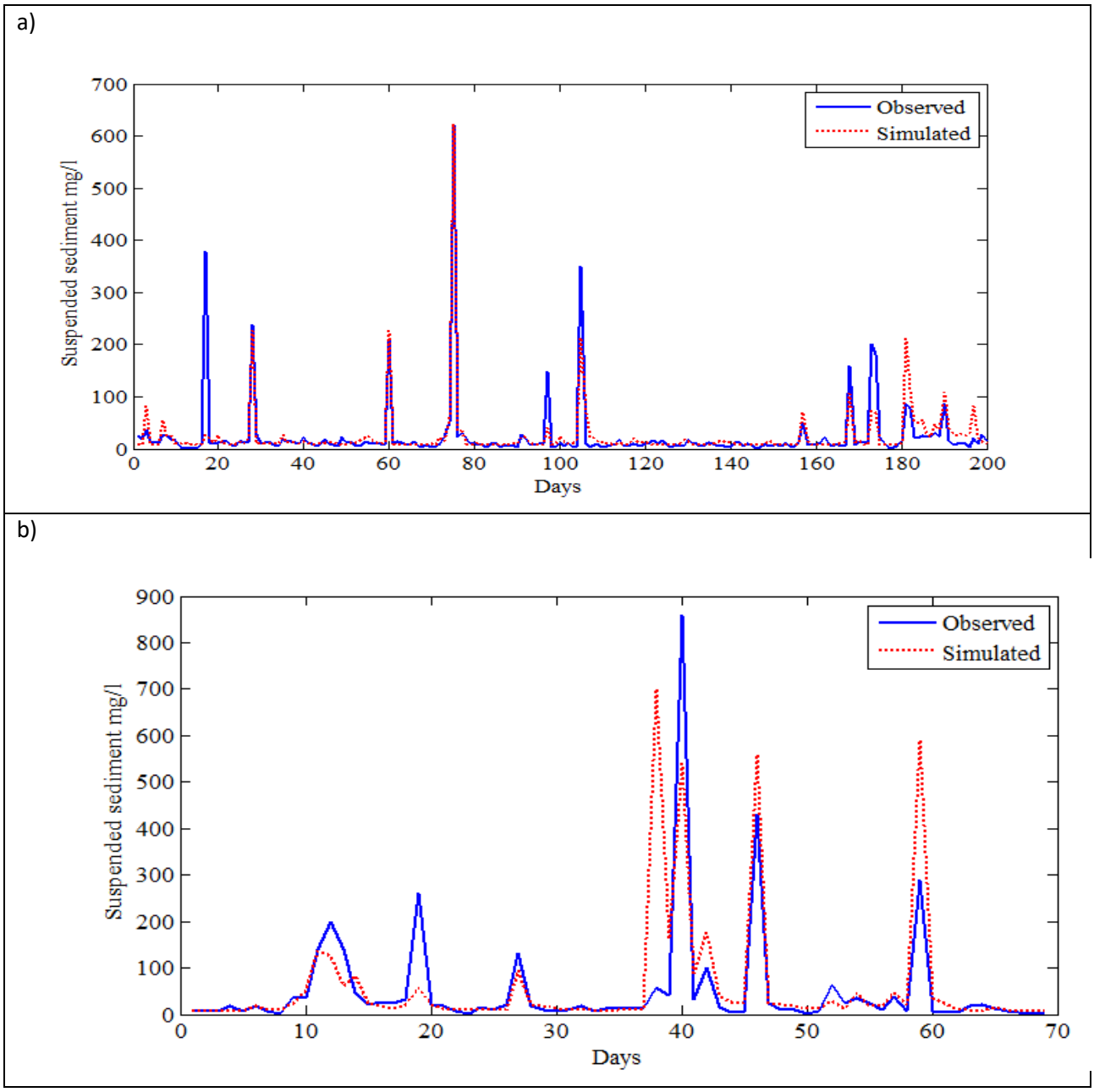

Figure 3 Observed versus modelled suspended sediment load from ANFIS during a) training b) validation periods

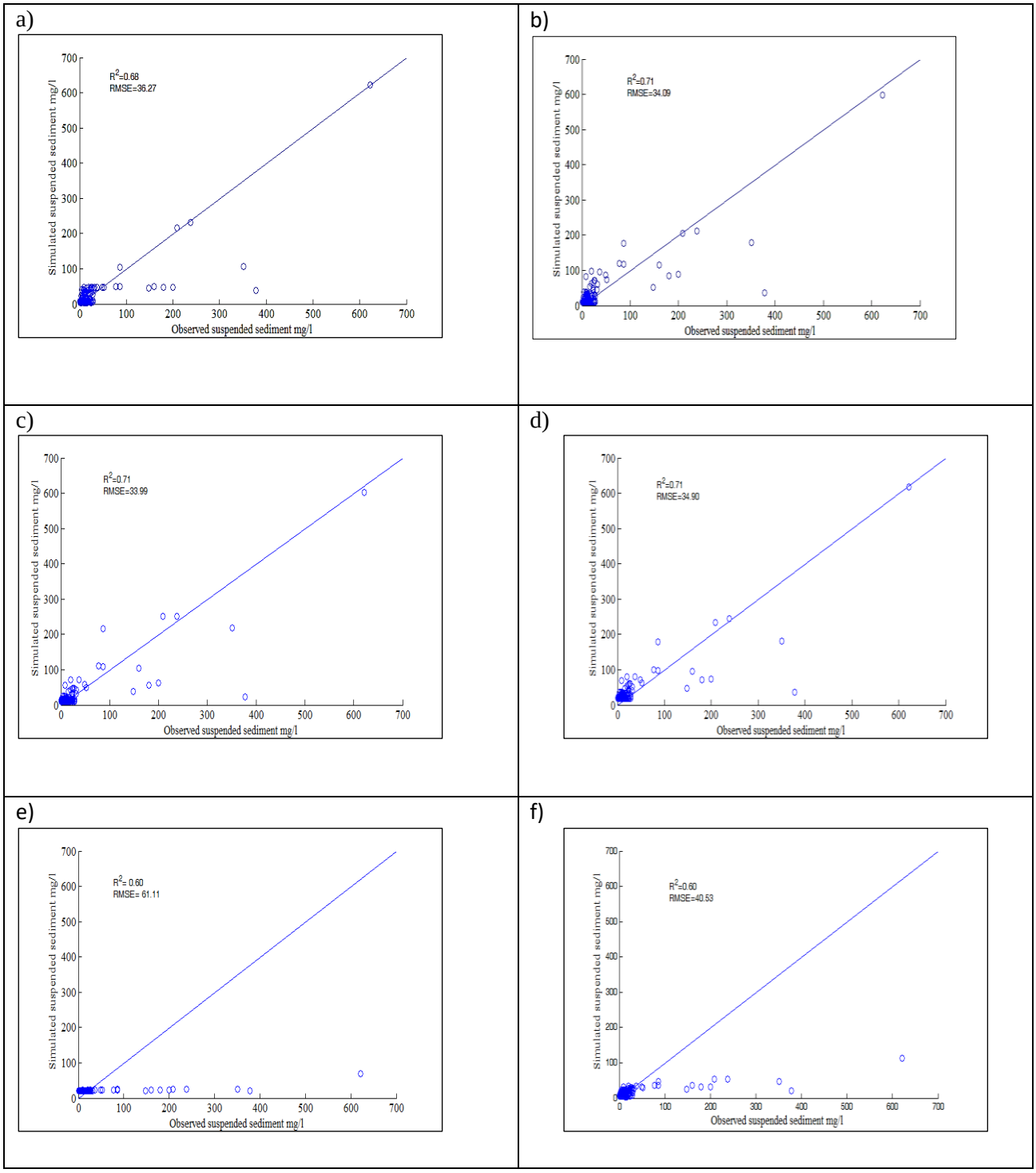

Figure 4 Comparison of observed and modelled suspended sediment in the training period from a) FF b) CFF c) PR d) LR e) GR f) SRC

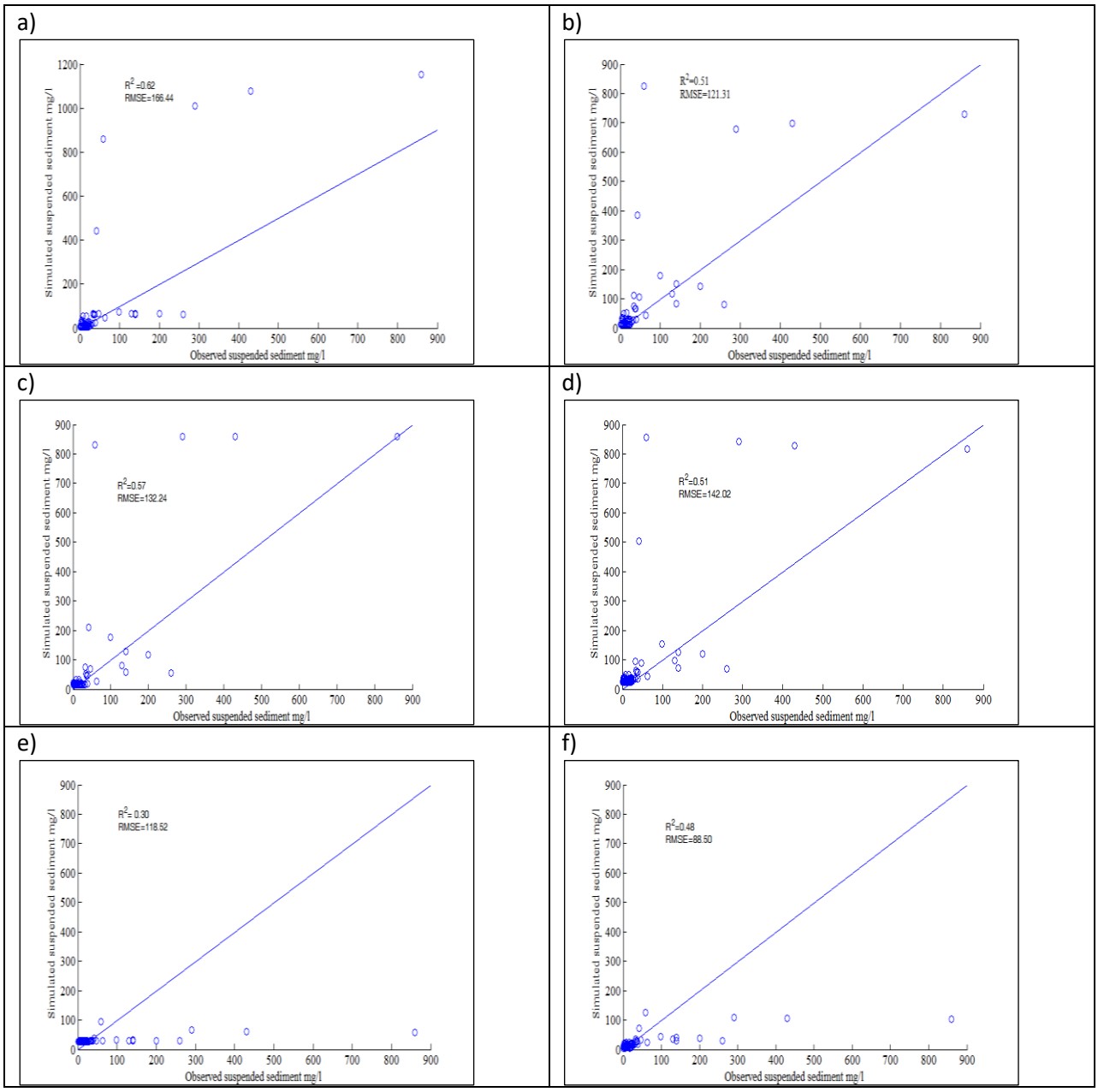

Figure 5 Comparison of observed and modelled suspended sediment in the validation period from a) FF b) CFF c) PR d) LR e) GR f) SRC

7.2 Estimating of suspended sediment load

In this study, the best structure of ANFIS was used to estimate the missing values of the SSL using the daily streamflow values of the study area from 1994 to 2010. The daily values of SSL (mg/l) were converted to ton/ha/yr using their corresponding streamflow discharges values and the catchment's area. Fig. 6 shows the temporal variation of the monthly-modelled SSL over the period 1993-2010 with the help of a box-whisker plot. The box-whisker plot pointed to the presence of many outliers, which implies that the SSL (ton/ha/yr) of some seasons is higher than those in others. This discrepancy was most likely due to other sources of point and non-point pollution because the catchment is characterized as a highly anthropogenic influenced area due to open pit mining. Fig. 7 shows the seasonal loads of suspended sediment over the period 1997-2006. The seasonal results confirm that in this region soil erosion was essentially a springtime process (March, April, and May) in most years (with value as high as 2.5 ton/ha) except a prominent summer process (Jun, July, and August) in 2010 (3.6 ton/ha). The higher value of suspended load during summer 2010 was most likely due to the high streamflow discharges that were recorded during this year (flood flow). Fig. 8 shows the yearly SSL over the period 1997-2006. These ten years were further used as a baseline period to investigate the deviation of future period's loads (2021-2030 and 2041-2050). Loads were varied from year to year. However, the yearly load ranges from 0.82 ton/ha in 2007 which was recorded as dry year to 17.25 ton/ha in 2010. Suspended sediment yield is expected to increase/decrease over the years depending on the major factors controlling sediment transport capacity i.e. streamflow and rainfall.

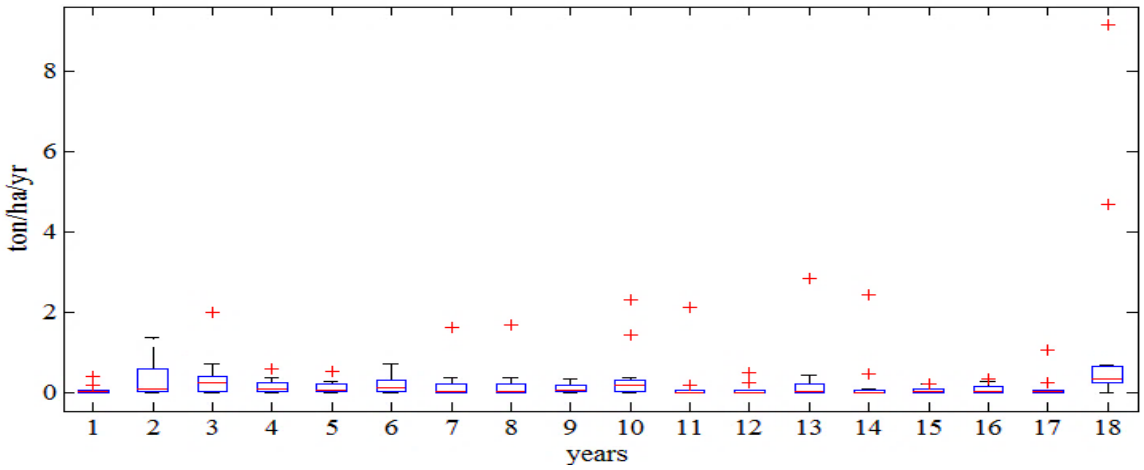

Figure 6 Temporal variation of suspended sediment load ton/ha/yr over period 1993-2010 (1 to 18)

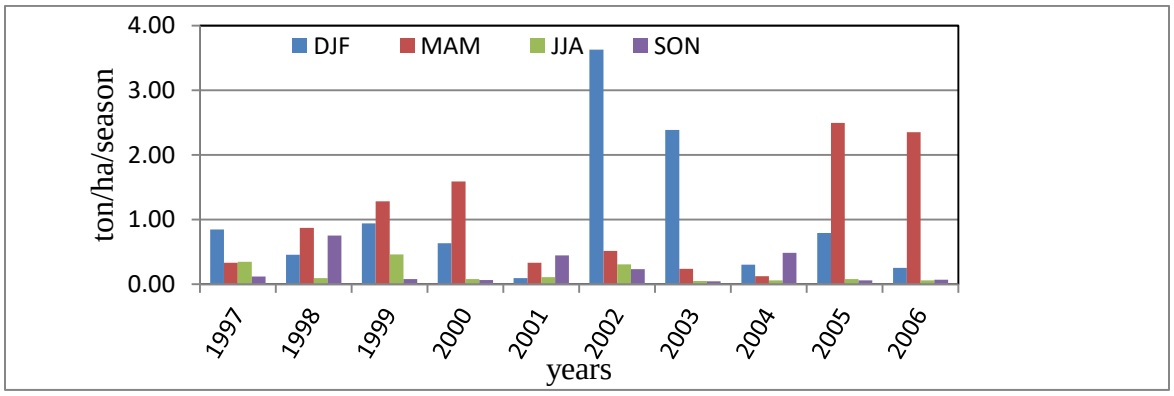

Figure 7 Seasonal in-stream loads of sediments from the upper reach of the Spree River watershed. DJF: December, January, February; MAM: March, April, May; JJA: June, July, August; SON: September, October, November

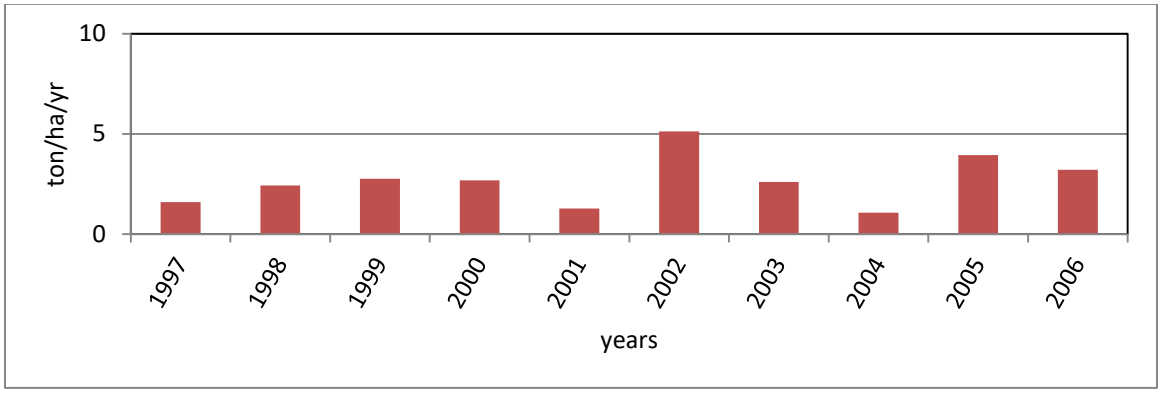

Figure 8 Yearly loads of suspended sediment as calculated from ANFIS in the upper reach of the Spree River

7.3 Swat calibration and validation

Two objective functions were used to assess the performance of SWAT model: R^2 and Nash and Sutcliffe coefficient efficiency (ENC). In addition, the P factor (the percentage of measured data surrounded by the 95% prediction uncertainty (95PPU)) and R factor (which is the average thickness of the 95PPU divided by the standard deviation of the measurements) were used to assess the simulation uncertainty. Figures 9 and 10 show the daily observed versus modelled streamflow from the SWAT model during the calibration and validation, respectively. SWAT underestimated the peak values along the two periods. This might be attributed to the assumption that the water percolates into deep aquifer is excluded from the simulation

process. However, during the calibration period (1997–2006), R^2 was 0.53 and the ENC coefficient is 0.53. During the validation period (2007–2010); the R^2 coefficient was 0.57 and the ENC coefficient is 0.54. SWAT shows a satisfactory performance in simulating daily stream flow in the upper reach of the Spree River, P factor and R factor were equal to 54 % and 36%, respectively during the calibration. During the validation, the P factor decreased to 40 % and the R factor to 31 %. However, the positive results during calibration and validation proved the reliability of the SWAT model to be used in further analysis i.e. predicting the impacts of climate changes on river flow.

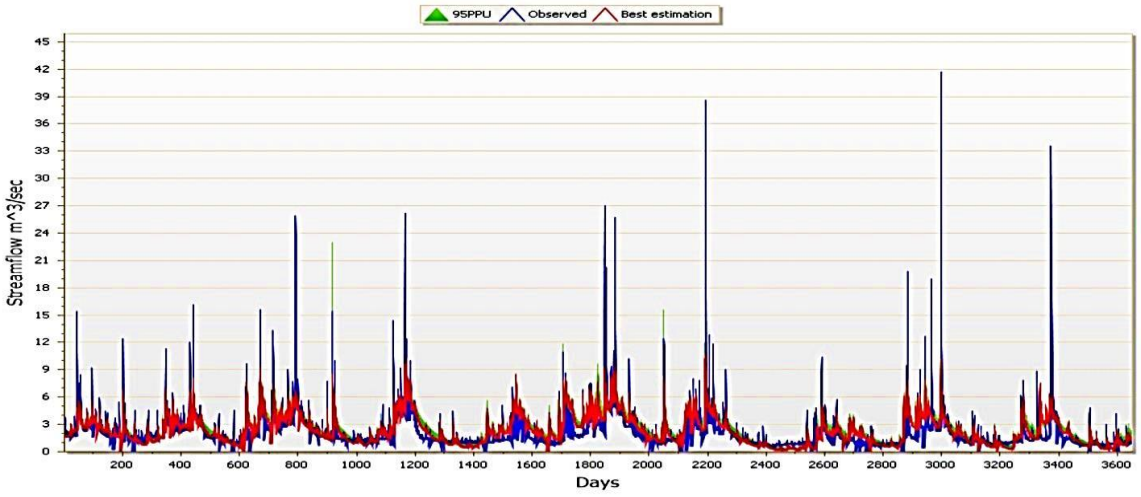

Figure 9 Observed versus modelled daily streamflow from SWAT during the calibration (1997-2006)

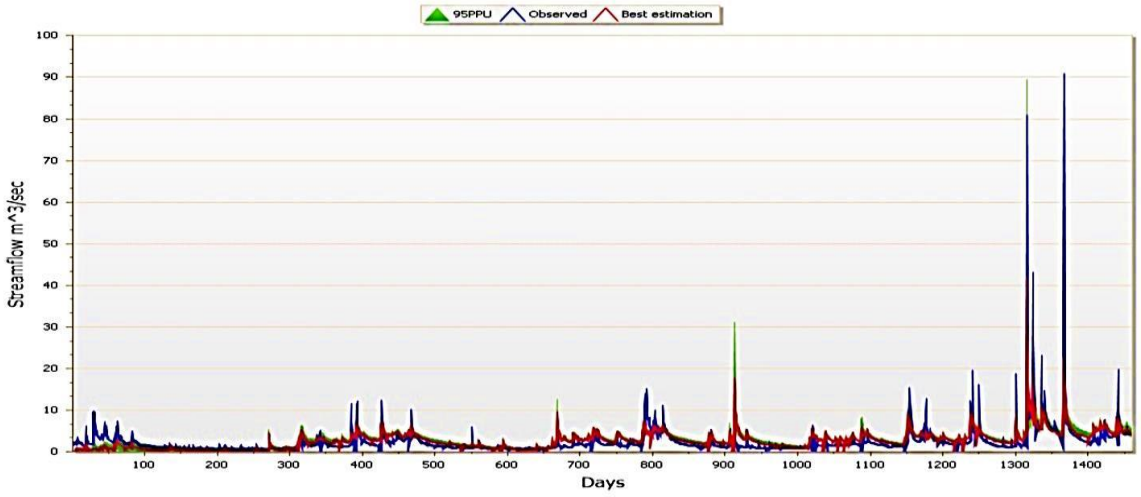

Figure 10 Observed versus modelled daily streamflow from SWAT during the validation (2007-2010)

7.4 Impact of climate change on suspended sediment

Figure 11 shows the relative change in seasonal suspended load during 2021-2030 and 2041-2050 in the study area. As it can be seen from Figure 11, the maximum reduction might occur in winter seasons (December-January-February) during 2021-2030 with 84.25%. A maximum reduction in period 2041-2050 was estimated to occur in spring season (March-April-May) with 75.60%. This decrease in sediment load corresponds to the prospective decrease in streamflow during the above periods that the catchment might undergo (Al-Mukhtar et al. 2014). Obviously, the effects of climate change are remarkable on the seasonal phases; which suggest that the seasonal climate variations are considerable in affecting future suspended sediment yield. The reduction in sediment load undoubtedly will have benefits in terms of pollutants transport, such as phosphorus and nutrients, because the transfer of phosphorus and metals from soils to surface waters is greatly affected by suspended sediment load. On the contrary, an increase in sediment load was projected in summer season (Jun-July-August) during 2041-2050 of 25%. This is attributed to the potential flood events that might occur. In other words, 50% of the annual precipitation occurs during the summer season in this area. Figure 12 shows the seasonal sediment load over period 2021-2030. It can be noticed from Figure 12 that the maximum sediment load was forecasted during March-April-May in 2026 and 2030 of values 0.49 and 0.56 ton/ha, respectively, which in turn interpreted the maximum yearly sediment load in these two years. During the period 2041-2050, the higher value of seasonal suspended load was forecasted to be 1 ton/ha in December-January-February in 2043 and 2046 as shown in Figure 13. A higher yearly value was forecasted with 2.8 ton/ha in 2046. An increase in future winter temperature (as predicted from A1B realization) effects on snowmelt in this region and ultimately on soil erosion, hence could explain why the higher values are projected in winter season. However, obviously, the impacts of climate changes will be more mitigated in 2041-2051 than in 2021-2030, which in turn might be attributed to the type of greenhouse emission scenario used in this evaluation. The overall relative change in yearly sediment load to the reservoir with respect to the baseline period (1997-2006) was projected to be 76% during 2021-2030 and 57% during 2041-2050. However, the results of this study should be cautiously considered due to the inherent uncertainties in evaluating climate change impacts on sediment yield, i.e., emission scenarios, global climatic projections, and model simulations.

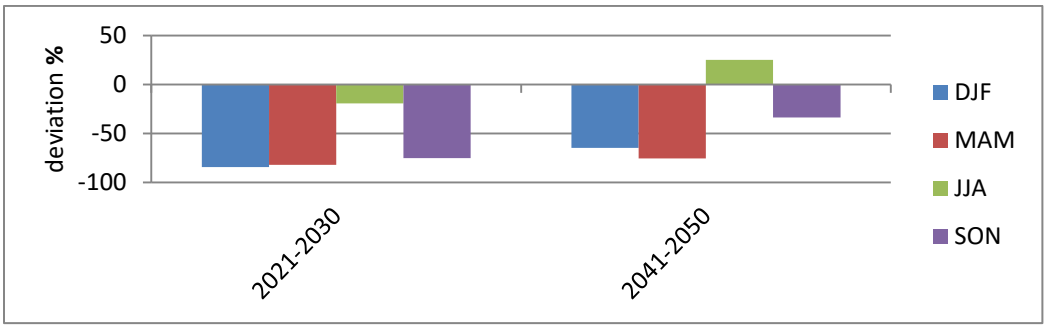

Figure 11 Relative changes in seasonal sediment yield for 2021-2030 and 2041-2050

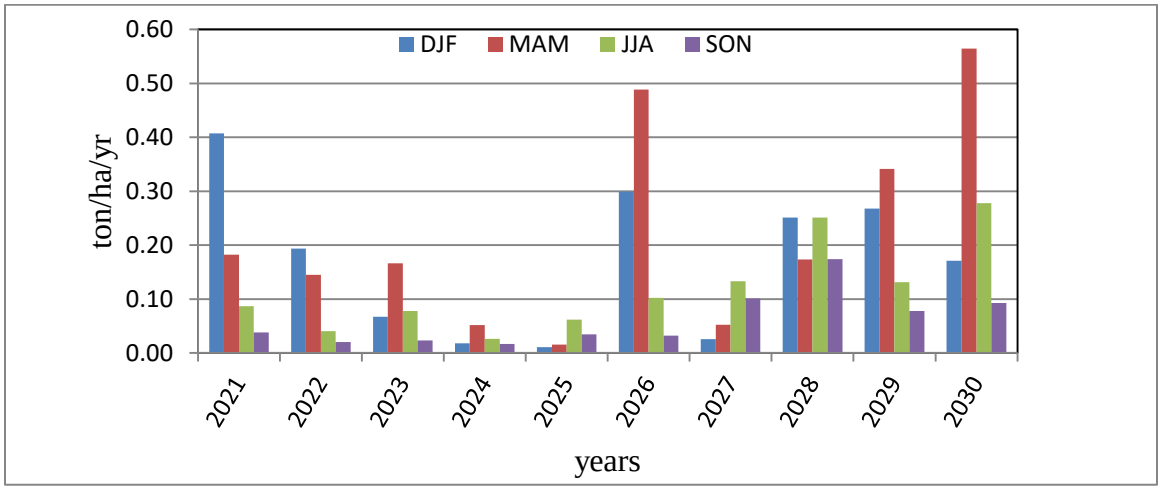

Figure 12 Seasonal sediment loads for 2021-2030

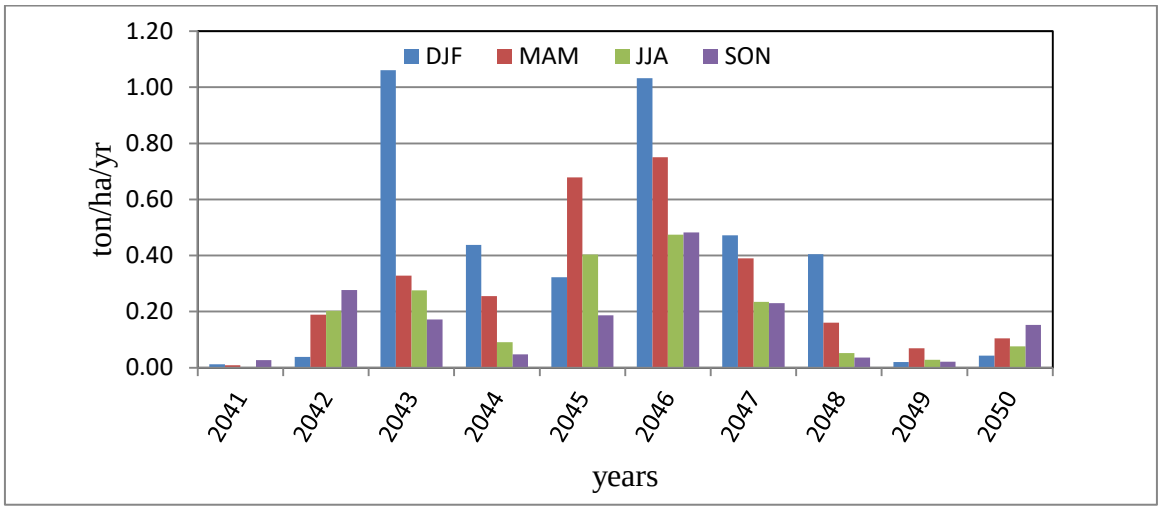

Figure 13 Seasonal sediment loads for 2041-2050

8 Conclusion

A novel methodology was used to assess the consequences of climate changes on SSL in the upper reach of the Spree River in Germany. Data from the Spree River in Germany was employed for this purpose. At first, the study evaluated and compared ANFIS, artificial neural networks and statistical regression analysis (SRC), to identify the optimal method that is capable to model the dependent suspended sediment concentration using streamflow as independent variable. Subsequently, the optimal AI structure was employed to estimate future SSL using estimated future discharges obtained from an integration of SWAT with a regional climate change model.

A comparison of the modeled suspended sediment concentration values with known records showed that the top performing method was the ANFIS. Thus, the ANFIS model has the priority in preference to the others neural network methods to be used as predictor of suspended sediment load in this area. The highest estimation accuracy of the ANFIS could be attributed to the non-linear characteristics, which can help in detecting and capturing non-linear features of SSL phenomenon (Kisi et al. 2009). On the opposite side, it is clear that the LR, FF, CFF, PR, RB, GR were not able to capture the behaviour of the observed sediment load series as accurate as the ANFIS. Rajaee et al. (2009) pointed out that “in contrast to regression-based models, intelligence-based models use the advantage of multiple adjustable parameters and configurations; therefore, they are prone to problems of over fitting”. However, results of this study prove the potential ability of ANFIS to model the complex nonlinear dynamic relationship such as that between discharge and suspended sediment load. Moreover, the findings from this study highlight the potentiality of this method to model other complex hydrologic relationships. It was found that the suspended sediment loads in the upper reach of the Spree River are greatly affected by outliers; suggesting that this area necessitates more frequent monitoring in terms of pollutants concentrations. It was also concluded that the amounts of suspended load are varied over the years with maximum load in 2010 and minimum in 2007. Moreover, it was concluded that the area might witness reduction in sediment load to Bautzen reservoir in the near future due to the impact of climate changes. This study could be of use to provide a better insight for stakeholders about the amounts of sediment load in this region. Hence, a better vision on risk analysis.

Acknowledgment

The author is grateful to the Ministry of Higher Education and Scientific Research in Iraq (MOHESR) represented by University of Technology in Baghdad for their support during conducting this study.

References

Abbaspour, K.C., Johnson, C.A., van Genuchten, M.T., 2004. Estimating uncertain flow and transport parameters using a sequential uncertainty fitting procedure. Vadose Zone J. 3, 1340–1352.

Abbaspour, K.C., Yang, J., Maximov, I., Siber, R., Bogner, K., Mieleitner, J., Zobrist, J., Srinivasan, R., 2007. Modelling of hydrology and water quality in the pre-alpine/alpine Thur watershed using SWAT. J. Hydrol. 333, 413–430.

Afan, H.A. et al., 2016. Past, present and prospect of an Artificial Intelligence (AI) based model for sediment transport prediction. *Journal of Hydrology*, 541, pp.902–913.

Al-Mukhtar, M., 2016. Modelling the root zone soil moisture using artificial neural networks, a case study. *Environmental Earth Sciences*, 75(15), p.1124.

Al-Mukhtar, M., Dunger, V. & Merkel, B., 2014. Assessing the Impacts of Climate Change on Hydrology of the Upper Reach of the Spree River: Germany. *Water Resources Management*, 28(10), pp.2731–2749.

Alp, M. & Cigizoglu, H., 2007. Suspended sediment load simulation by two artificial neural network methods using hydrometeorological data. *Environmental Modelling & Software*, 22(1), pp.2–13.

ASCE Task Committee on Application of Artificial Neural Networks in Hydrology, 2000a. Artificial neural networks in hydrology. I: Preliminary concepts. *Journal of Hydrologic Engineering*, 5(2), pp.115–123.

ASCE Task Committee on Application of Artificial Neural Networks, 2000b. Artificial neural networks in hydrology. II: hydrologic applications. *Journal of Hydrologic Engineering*, 5(2), pp.124–137.

Beale, M.H., Hagen, M.T. & Demuth, H.B., 2012. *Neural Network Toolbox: users guide*.

Chen, X.Y., Chau, K.W. & Busari, A.O., 2015. A comparative study of population-based optimization algorithms for downstream river flow forecasting by a hybrid neural network model. *Engineering Applications of Artificial Intelligence*, 46, pp.258–268.

Cigizoglu, H.K., 2005. Generalized regression neural network in monthly flow forecasting. *Civil Engineering and Environmental Systems*, 22(2), pp.71–81.

Cigizoglu, H.K. & Alp, M., 2006. Generalized regression neural network in modelling river sediment yield. *Advances in Engineering Software*, 37(2), pp.63–68.

Daliakopoulos, I.N., Coulibaly, P. & Tsanis, I.K., 2005. Groundwater level forecasting using artificial neural networks. *Journal of Hydrology*, 309(1–4), pp.229–240.

Dawson, C.W. & Wilby, R.L., 2001. Hydrological modelling using artificial neural networks. *Progress in Physical Geography*, 25(1), pp.80–108.

Dumedah, G., Walker, J.P. & Chik, L., 2014. Assessing artificial neural networks and statistical methods for infilling missing soil moisture records. *Journal of Hydrology*, 515, pp.330–344.

El-Shafie, A., Taha, M.R. & Noureldin, A., 2007. A neuro-fuzzy model for inflow forecasting of the Nile river at Aswan high dam. *Water Resources Management*, 21(3), pp.533–556.

Feng, L.-H. & Lu, J., 2010. The practical research on flood forecasting based on artificial neural networks. *Expert Systems with Applications*, 37(4), pp.2974–2977.

Feng, L. & Hong, W., 2008. On hydrologic calculation using artificial neural networks. *Applied Mathematics Letters*, 21, pp.453–458.

Fernando, D.A.K. & Jayawardena, A.W., 1998. Runoff forecasting using RBF networks with OLS algorithm. *Journal of hydrologic engineering*, 3(3), pp.203–209.

Flood, I. & Kartam, N., 1994. Neural networks in civil engineering. II: Systems and application. *Journal of Computing in Civil Engineering*, 8(2), pp.149–162.

Hagan, M.T., Demuth, H.B. & Beale, M.H., 1996. *Neural network design*,

Jain, S.K., 2001. Development of integrated sediment rating curves using ANNs. *Journal of hydraulic engineering*, 127(1), pp.30–37.

Jang, J.-S.R., Sun, C.-T. & Mizutani, E., 1997. Neuro-fuzzy and soft computing; a computational approach to learning and machine intelligence.

Jang, J.R., 1993. ANFIS : Adap tive-Ne twork-Based Fuzzy Inference System.

Kerem Cigizoglu, H. & Kisi, O., 2006. Methods to improve the neural network performance in suspended sediment estimation. *Journal of Hydrology*, 317(3–4), pp.221–238.

Kisi, O. et al., 2009. Adaptive neuro-fuzzy computing technique for suspended sediment estimation. *Advances in Engineering Software*, 40(6), pp.438–444.

Kisi, O. & Kerem Cigizoglu, H., 2007. Comparison of different ANN techniques in river flow prediction. *Civil Engineering and Environmental Systems*, 24(3), pp.211–231.

Kisi, O. & Zounemat-Kermani, M., 2016. Suspended Sediment Modeling Using Neuro-Fuzzy Embedded Fuzzy c-Means Clustering Technique. *Water Resources Management*, 30(11), pp.3979–3994.

Lallahem, S. et al., 2005. On the use of neural networks to evaluate groundwater levels in fractured media. *Journal of Hydrology*, 307(1–4), pp.92–111.

Van Liew, M.W., Arnold, J.G. & Garbrecht, J.D., 2003. Hydrologic simulation on agricultural watersheds: Choosing between two models. *Transactions of the ASAE*, 46(6), pp.1539–1551.

Luk, K.C., Ball, J.E. & Sharma, a., 2000. A study of optimal model lag and spatial inputs to artificial neural network for rainfall forecasting. *Journal of Hydrology*, 227(1–4), pp.56–65.

Luk, K.C., Ball, J.E. & Sharma, a., 2001. An application of artificial neural networks for rainfall forecasting. *Mathematical and Computer Modelling*, 33, pp.683–693.

Maier, H.R. & Dandy, G.C., 2000. Neural networks for the prediction and forecasting of water resources variables: A review of modelling issues and applications. *Environmental Modelling and Software*, 15, pp.101–124.

Maiti, S. & Tiwari, R.K., 2014. A comparative study of artificial neural networks, Bayesian neural networks and adaptive neuro-fuzzy inference system in groundwater level prediction. *Environmental Earth Sciences*, 71(7), pp.3147–3160.

Mason, J.C., Price, R.K. & Tem'Me, A., 1996. A neural network model of rainfall-runoff using radial basis functions. *Journal of Hydraulic Research*, 34(4), pp.537–548.

McCuen, Ricahard, H., 2002. *Modelling Hydrological Change: Statistical Methods*. Washington D.C.

Minns, A.W. & Hall, M.J., 1996. Artificial neural networks as rainfall-runoff models. *Hydrological Sciences Journal*, 41(3), pp.399–417.

Moriasi, D.N. et al., 2007. Model evaluation guidelines for systematic quantification of accuracy in watershed simulations. *American Society of Agricultural and Biological Engineers*, 50(3), pp.885–900.

Nagy, H.M., Watanabe, K. & Hirano, M., 2002. Prediction of sediment load concentration in rivers using artificial neural network model. *Journal of Hydraulic Engineering*, 128(6), pp.588–595.

Palani, S., Liong, S.Y. & Tkalich, P., 2008. An ANN application for water quality forecasting. *Marine Pollution Bulletin*, 56(9), pp.1586–1597.

Quilbé, R. et al., 2006. Selecting a calculation method to estimate sediment and nutrient loads in streams: Application to the Beaurivage River (Québec, Canada). *Journal of Hydrology*, 326(1–4), pp.295–310.

Rai, R.K. & Mathur, B.S., 2008. Event-based sediment yield modeling using artificial neural network. *Water Resources Management*, 22(4), pp.423–441.

Rajaee, T. et al., 2009. Daily suspended sediment concentration simulation using ANN and neuro-fuzzy models. *Science of the Total Environment*, 407(17), pp.4916–4927.

Santhi, C. et al., 2002. Validation of the SWAT model on a large river basin with point and nonpoint sources. *Journal of the American Water Resources Association (JAWRA)*, 37(5), pp.1169–1188.

Shiau, J.-T. & Chen, T.-J., 2015. Quantile Regression-Based Probabilistic Estimation Scheme for Daily and Annual Suspended Sediment Loads. *Water Resources Management*, 29(8), pp.2805–2818.

Singh, K.P. et al., 2009. Artificial neural network modeling of the river water quality-A case study. *Ecological Modelling*, 220(6), pp.888–895.

Tayfur, G., 2002. Artificial neural networks for sheet sediment transport. *Hydrological Sciences Journal*, 47(6), pp.879–892.

Tokar, A.S. & Johnson, P.A., 1999. Rainfall-runoff modeling using artificial neural networks. *Journal of Hydrologic Engineering*, 4(3), pp.232–239.

Valverde Ramírez, M.C., De Campos Velho, H.F. & Ferreira, N.J., 2005. Artificial neural network technique for rainfall forecasting applied to the São Paulo region. *Journal of Hydrology*, 301(1–4), pp.146–162.

Wen, C. & Lee, C., 1998. A neural network approach to multiobjective optimization for water quality management in a river basin. *Water Resources Research*, 34(3), pp.427–436.

Winchell M, Srinivasan R, Di Luzio M, Arnold JG, 2010 ArcSWAT interface for SWAT 2009 user's guide. Blackland Research Center, Texas Agricultural Experiment Station and Grassland, Soil andWater Research Laboratory, USDA Agricultural Research Service, Temple, Texas